

Vibration-based damage monitoring of harbor caisson structure with damaged foundation-structure interface

So-Young Lee¹, Khac-Duy Nguyen¹, Thanh-Canh Huynh¹, Jeong-Tae Kim^{*1},
Jin-Hak Yi² and Sang-Hun Han²

¹*Department of Ocean Eng., Pukyong National University, Busan, Korea*

²*Coastal Development & Ocean Energy Research Dept.,*

Korea Institute of Ocean Science and Technology (KIOST), Ansan, Korea

(Received November 11, 2011, Revised July 30, 2012, Accepted August 17, 2012)

Abstract. In this paper, vibration-based methods to monitor damage in foundation-structure interface of harbor caisson structure are presented. The following approaches are implemented to achieve the objective. Firstly, vibration-based damage monitoring methods utilizing a variety of vibration features are selected for harbor caisson structure. Autoregressive (AR) model for time-series analysis and power spectral density (PSD) for frequency-domain analysis are selected to detect the change in the caisson structure. Also, the changes in modal parameters such as natural frequency and mode shape are examined for damage monitoring in the structure. Secondly, the feasibility of damage monitoring methods is experimentally examined on an un-submerged lab-scaled mono-caisson. Finally, numerical analysis of un-submerged mono-caisson, submerged mono-caisson and un-submerged interlocked multiple-caissons are carried out to examine the effect of boundary-dependent parameters on the damage monitoring of harbor caisson structures.

Keywords: harbor caisson; foundation-structure interface; damage monitoring; autoregressive model; power spectral density; modal parameters

1. Introduction

Caisson structures have been used for breakwater and quay wall, and also applied to foundation construction area for in-land structures. Caisson breakwater stands on foundation mound constructed on seabed and it is mostly gravity-type structure stabilized by its own weight. Most of harbor caisson body is submerged and it is mainly designed to keep tranquility in harbor by dissipating wave energy from open sea (Allen 1998). Over the last two decades, many caisson breakwaters have been constructed in Korea. During the same period, genesis frequency of large-scale typhoon and storm surge has increased due to global warming. Consequently, those structures have experienced a lot of extreme events that might cause unwanted geometrical and mechanical changes, eventually deviated from the as-built designs. For instance, typhoon Maemi hit the southern part of the Korean Peninsula in 2003 and it resulted in severe damages such as failure of caisson structure, loss of foundation mound, differential settlement, etc. As an effort to deal with this problem, Korean Ministry of Land, Transport and Maritime Affairs established the standard for safety diagnosis of gravity-type

*Corresponding author, Professor, E-mail: idis@pknu.ac.kr

harbor structures.

Upon repeatedly experiencing wave forces that are stronger than design wave force, the structure cannot be ensured for its safety. Local potential damages such as cavity on foundation mound or backfill cause weakening the global structural functionality upon subjected to extreme loads. For harbor caisson structure, therefore, suitable damage monitoring should be performed to detect global damage and local defect. Global damage includes settlement, overturning and sliding of the structure, which are rather indicative to open-air visual observation. Meanwhile, local defect includes scouring and disturbance in foundation, which are not obvious to visual observation. Significant damage in harbor caisson occurs mostly on foundation-structure interface (i.e., foundation mound) since local defects occurred in the foundation mound are eventually transformed into global damages when experiencing extreme wave forces. Therefore, there is a need to develop damage monitoring methods for detecting local damage in the foundation-structure interface of the caisson structure.

So far, many research studies have been performed for vibration-based damage monitoring of civil structures (Doebling *et al.* 1998, Jang *et al.* 2010). Many researchers have attempted to detect damage in structures using dynamic characteristics (Shi *et al.* 1998, Brownjohn *et al.* 2001, Kwon and Shin 2006, Catbas *et al.* 2008, Isemoto *et al.* 2011). Also, many researchers have worked on developing damage detection methods such as modal sensitivity method, modal flexibility method, genetic algorithm, neural network, etc (Wu *et al.* 1992, Kim and Stubbs 1995, Atkan *et al.* 1997, Levin and Lieven 1998, Yun and Bahng 2000, Yun *et al.* 2009).

Up-to-date research studies, however, have focused mostly on in-land structures such as bridge and building but only a few research efforts have been made for harbor structures. A few researchers have studied on vibration response analyses of soil-structure or fluid-soil-structure interactions in harbor caisson structures (Yang *et al.* 2001, Kim *et al.* 2005). Specifically, a few researchers have attempted to identify experimental modal parameters of wharf structures by using micro-vibration signals produced by tides, wind, wave and micro-tremors (Boroschek *et al.* 2011) and to estimate damage in harbor caisson structures by using changes in experimental modal parameters (Lee *et al.* 2011). Despite those research attempts, however, there still exist several research needs on harbor caisson structures: (1) to monitor vibration responses of the caisson with limited accessibility, (2) to analyze the feasibility of utilizing a variety of vibration features for detecting damage occurrence in the caisson, (3) to specifically identify sensitive motions (e.g., vibration modes) with respect to damage in the caisson's foundation-structure interface, and 4) to assess the safety of the caisson on the basis of the damage monitoring results.

Specifically considering the real conditions of the harbor caisson structures, moreover, vibration features and damage monitoring methods should be examined for the following two issues: (1) real caisson structures are partially submerged in the sea water, and (2) a harbor structure system consists of multiple segments of caisson units. Related to the first issue, Wang *et al.* (2006) reported that dynamic parameters of caisson structure are changed due to partially submerged condition. From their experiment, natural frequency decreases and damping ratio increases according to water-level rise. For the second issue, caissons are usually designed with shear keys to prevent them from shear motion and to resist against the wave forces which act normal to the front wall. Vibration response of a caisson segment can be propagated into others since adjacent segments are interconnected each other by shear keys.

In this paper, vibration-based methods to monitor damage in foundation-structure interface of harbor caisson structure are presented. Firstly, vibration-based damage monitoring methods utilizing a variety of vibration features are selected for harbor caisson structure. Autoregressive (AR) model for time-

series analysis and power spectral density (PSD) for frequency-domain analysis are selected to identify the change in the caisson structure by using acceleration responses measured from a single point. Also, natural frequency and mode shape changes are examined for damage monitoring in the structure. Secondly, the feasibility of damage monitoring methods is experimentally examined on an un-submerged lab-scaled mono-caisson. Considering above-mentioned aspects on real situation of harbor caissons, numerical studies are also performed on un-submerged mono-caisson, submerged mono-caisson, and un-submerged interlocked multiple-caissons to examine the effect of boundary-dependent parameters on the damage monitoring in harbor caisson structures.

2. Vibration-based damage monitoring methods

2.1 Autoregressive model-based damage monitoring

Autoregressive (AR) model is one of the time series analysis methods that forecasts future response from past time history response. Sohn and Farrar (2001) have successfully applied the AR model to detect damage of structure. For estimating acceleration response, AR model is defined as follows

$$\ddot{x}(t) = \sum_{j=1}^a \varphi_j \ddot{x}(t-j) + e(t) \quad (1)$$

where $\ddot{x}(t)$ is the time history of acceleration at time step t , φ_j is the j th AR coefficient, a is the order of AR model, and $e(t)$ is the residual error. The change in AR coefficients represents the change in structural parameters. To analyze the change of AR coefficients due to the structural change, Mahalanobis-squared-distance (MSD) is calculated as follow

$$D_\zeta = (\varphi_\zeta - \bar{\varphi})^T \mathbf{S}^{-1} (\varphi_\zeta - \bar{\varphi}) \quad (2)$$

where D_ζ is the MSD value, φ_ζ is the AR coefficient vector (outlier), $\bar{\varphi}$ is the mean vector of n sets of AR coefficient, and \mathbf{S} is the covariance matrix of n sets of AR coefficient. The variation of MSD quantitatively indicates the variation of AR coefficients due to damage. The number of set, n is determined by partial autocorrelation function of the first acceleration sample in intact state. It is noted that the number of set, n , should be larger than the order of AR model, a .

For damage alarming, control chart analysis is performed to discriminate outlying events from the MSD values. The alarming threshold is determined by upper control limit (UCL) as follows

$$UCL_D = \mu_D + 3\sigma_D \quad (3)$$

where μ_D and σ_D are the mean and the standard deviation of the MSD values, respectively. The occurrence of damage is indicated when the MSD values are beyond the bound of the UCL; otherwise, there is no indication of damage occurrence.

As summary, autoregressive model-based damage monitoring method is performed in initialization and monitoring phases. The initialization phase includes the following four steps: firstly, n sets of vibration responses are measured from undamaged caisson structure as the data for reference state; secondly, features of AR model (e.g., AR coefficients, φ_j) and its mean vector and covariance matrix are calculated by Eq. (1); thirdly, MSD values for the undamaged state are calculated by Eq.

(2); and finally, UCL value is calculated by Eq. (3) from MSD values for undamaged state. The monitoring phase includes the four steps: firstly, vibration responses are measured from the target caisson in which structural safety and stability should be estimated; secondly, the features of AR model for the target caisson are calculated by Eq. (1); thirdly, MSD values are calculated by Eq. (2); and finally, damage occurrence is indicated by any outliers triggered by UCL value.

2.2 Power spectral density-based damage monitoring

Assume there are two acceleration signals, $x(t)$ and $y(t)$, measured before and after a damaging episode, respectively. The corresponding power spectral densities, S_{xx} and S_{yy} , are calculated from Welch's procedure as (Bendat and Piersol 2003)

$$S_{xx}(f) = \frac{1}{n_d T} \sum_{i=1}^{n_d} |X_i(f, T)|^2 \quad (4a)$$

$$S_{yy}(f) = \frac{1}{n_d T} \sum_{i=1}^{n_d} |Y_i(f, T)|^2 \quad (4b)$$

where X and Y are the frequency response transformed from correspondent acceleration signal; n_d is the number of divided segment; and T is the data length of divided segment.

The correlation coefficient (CC) of PSDs represents the linear identity between the two PSDs obtained before and after a damage event, as follows

$$\rho_{XY} = \frac{E[S_{xx}S_{yy}] - \mu_{S_{xx}}\mu_{S_{yy}}}{\sigma_{S_{xx}}\sigma_{S_{yy}}} \quad (5)$$

where $E[\cdot]$ is the expectation operator, and $\sigma_{S_{xx}}$ and $\sigma_{S_{yy}}$ are the standard deviations of PSDs of acceleration signals measured before and after damaging episode, respectively. If any damage occurs in target structure, its acceleration responses would be affected and, consequently, the decrement of CC can be a warning sign for the presence of damage.

For damage alarming, control chart analysis is also performed to discriminate damage events from the CC values. The alarming threshold is determined by lower control limit (LCL) as follows

$$LCL_{\rho} = \mu_{\rho} - 3\sigma_{\rho} \quad (6)$$

where μ_{ρ} and σ_{ρ} are the mean and the standard deviation of the CC values, respectively. The occurrence of damage is indicated when the CC values are beyond (i.e., less than) the bound of the LCL; otherwise, there is no indication of damage occurrence.

As summary, power spectral density-based damage monitoring method is performed in initialization and monitoring phases. The initialization phase is outlined in four steps: firstly, n sets of acceleration are measured from undamaged caisson; secondly, PSDs of acceleration signals are calculated by Eq. (4); thirdly, CC values for n sets of PSD are calculated by Eq. (5); and finally, LCL value is determined by Eq. (6). The monitoring phase is outlined as follows: firstly, acceleration signals are measured from the target caisson; secondly, PSDs of acceleration signals are calculated by Eq. (4); thirdly, CC values for the monitored state are calculated by Eq. (5); and finally, damage occurrence is indicated by any outliers triggered by the LCL value.

2.3 Modal parameter-based damage monitoring

Frequency domain decomposition (FDD) method (Otte *et al.* 1990, Yi and Yun 2004) is used to extract modal parameters such as natural frequency and mode shape. The singular values of the PSD function matrix $\mathbf{S}(\omega)$ are used to estimate the natural frequencies instead of the PSD functions themselves as follows

$$\mathbf{S}(\omega) = \mathbf{U}(\omega)^T \boldsymbol{\Sigma}(\omega) \mathbf{V}(\omega) \quad (7)$$

where $\boldsymbol{\Sigma}$ is the diagonal matrix consisting of the singular values (σ_i 's) and \mathbf{U} and \mathbf{V} are unitary matrices. Since $\mathbf{S}(\omega)$ is symmetric, \mathbf{U} becomes equal to \mathbf{V} . In this FDD method, the natural frequencies can be determined from the peak frequencies of the singular value, and the mode shapes are extracted from any one of the column vectors of $\mathbf{U}(\omega)$ at the corresponding peak frequencies. Generally the first singular value $\sigma_1(\omega)$ among σ_i 's ($i=1, \dots, N$) is used to estimate the modal parameters except in some special cases such as with two or more identical excitations.

Mode shapes measured before and after damaging episode are examined by modal assurance criterion (MAC). MAC provides a measure of the least-squares deviation or scatter of the points from the linear correlation (Ewins 2000).

$$\text{MAC}(\phi_i, \phi_i^*) = \frac{[\phi_i^T \phi_i^*]^2}{[\phi_i^T \phi_i][\phi_i^{*T} \phi_i^*]} \quad (8)$$

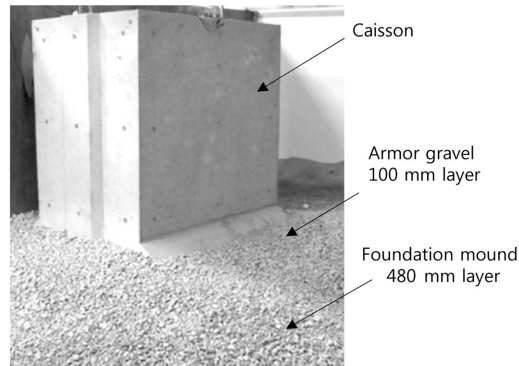
where ϕ_i and ϕ_i^* are the modal vectors which are extracted from acceleration signals measured before and after damaging episode, respectively. The MAC value provides to quantify the comparison between the two sets of mode shape data. In practice, a value of MAC close to the unity is expected if the two sets of mode shapes have no change due to damage; otherwise, the MAC value would decrease due to damage. This method can be utilized to obtain the information on what vibration modes are sensitive to special damage type or damage location. By considering the fact that the acceleration responses can be measured at the top of the real caisson structure, the FE model analysis is helpful to distinguish the types of modes without implementing many sensors.

3. Damage monitoring in lab-scale caisson

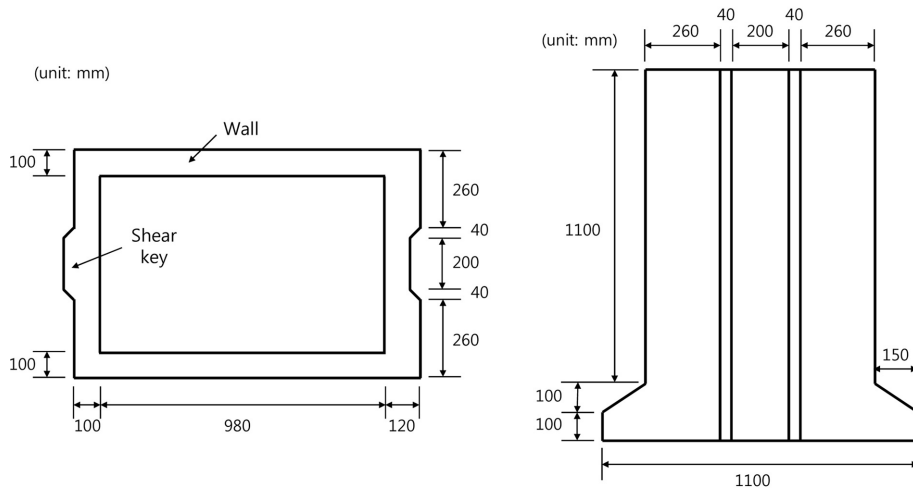
3.1 Experimental setup and dynamic test

In order to examine the feasibility of the vibration-based SHM techniques on indicating foundation-structure interface damage, dynamic tests on a lab-scale caisson were conducted. Fig. 1(a) shows an un-submersed lab-scale mono-caisson on test condition. The lab-scale caisson had approximately 1/20 size of real one. The width, length, and height were 1200 mm, 1100 mm, and 1300 mm, respectively. Detailed dimensions are shown in Fig. 1(b). As the experimental setup, the caisson was installed on the foundation mound which was constructed with 480 mm thick sand layer, and covered by 100 mm thick armor gravel layer. The setup was performed similar to harbor caissons at the real site.

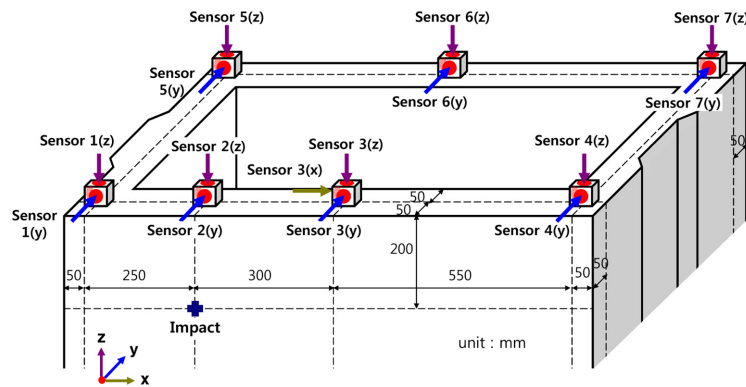
To measure vibration responses of the lab-scale caisson, fifteen accelerometers were installed along the x -, y -, and z -directions on top of the caisson, as shown in Fig. 1(c). An impact force, which has



(a) Lab-scale caisson on foundation



(b) Detailed dimensions of caisson



(c) Orientation of sensor and impact

Fig. 1 Experimental setup of lab-scale caisson

correspondent direction of incident wave, was applied perpendicularly to the front wall of caisson (i.e., y -direction) at the location denoted in Fig. 1(c). The amplitude and duration of impact excitation were randomly generated. Data acquisition system consisted of a signal conditioner, a terminal block, a

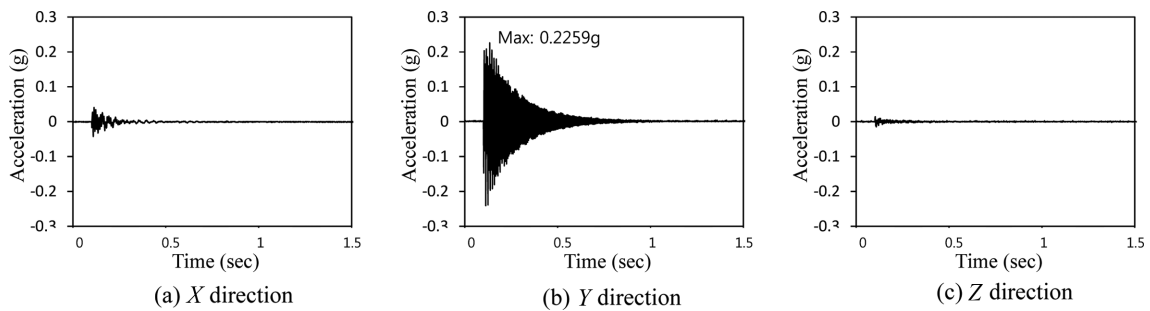


Fig. 2 Experimental acceleration signals of Sensor 3 on lab-scale caisson

DAQ card, and a laptop. Fig. 2 shows acceleration signals of Sensors 3 measured with 1 kHz sampling rate. The *y*-directional (along the wave action) and *z*-directional (vertical) acceleration responses are the largest (about 0.2259 g) and the smallest, respectively.

3.2 Damage monitoring in lab-scale caisson

3.2.1 Damage cases of foundation-structure interface

For experimental simulation of damage, it was assumed that scouring occurred at the foundation-structure interface under extreme external loading such as typhoon. Thus, several damages were inflicted with regarding to the loss of foundation mound. Fig. 3 illustrates damage cases of the foundation-structure interface. Foundation loss was inflicted in the model caisson system by removing damaged part of foundation-structure interface. In Damage 1, about 2.5% of armor gravel was removed as the incipient stage. In Damage 2, about 3.0% of armor gravel and about 1.6% of foundation mound were removed as moderate damage stage. In Damage 3, about 3.5% of armor gravel and 4.4% of foundation mound was removed as the most severe damage stage. For Damage 3, the damaged area was expanded to foundation-caisson contact region, and the amount of non-contact area was about 17% of bottom surface of the caisson. In the non-contact area, the foundation-structure interface lost supporting function for caisson structure.

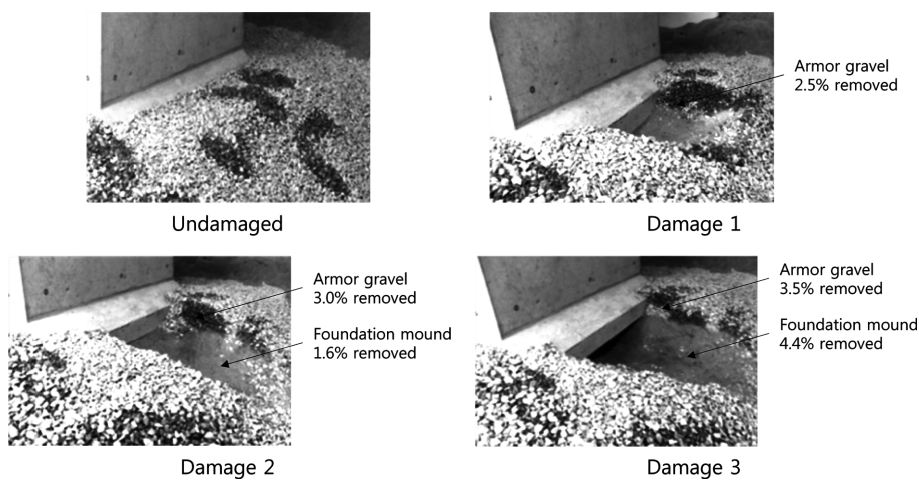


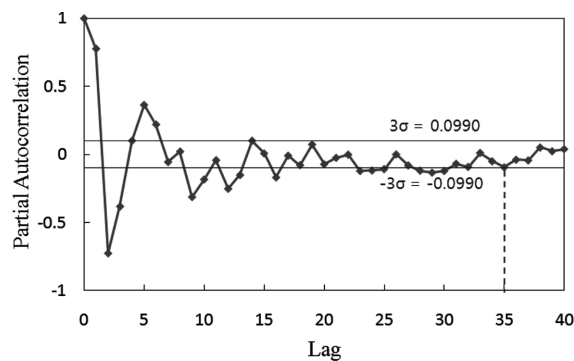
Fig. 3 Damage cases for lab-scale caisson

3.2.2 AR model-based damage monitoring

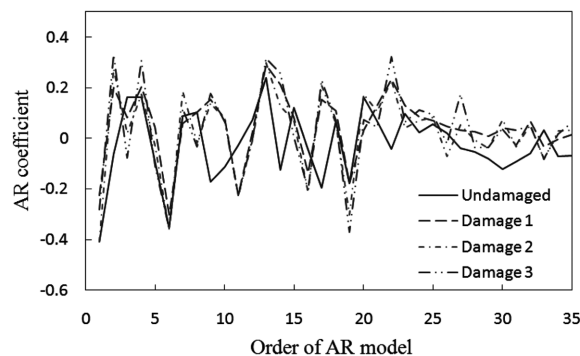
Acceleration responses from Sensor 3(x), Sensor 3(y) and Sensor 3(z) shown in Fig. 2(b) were utilized for AR model described in Eq. (1). In order to determine the order of AR model, partial autocorrelation analysis was carried out for the first acceleration data set under undamaged state. Partial autocorrelation is converged to zero as increase of lag. Three times of standard deviation (STD) was selected as criterion of convergence, in this study. As shown in Fig. 4(a), partial autocorrelation of acceleration signal is converged into three times of STD when lag is larger than 35.

In the initialization phase, AR coefficients of 50 acceleration data sets measured for undamaged state were calculated by Eq. (1). The mean vector and covariance matrix of AR coefficients were also computed as the database for reference state. Then, MSD value for each of the eight data sets was calculated by Eq. (2) and UCL value was determined from 8 MSD values of undamaged state by Eq. (3). In the monitoring phase, AR coefficients of acceleration signals were calculated by Eq. (1) from the three damaged states. Fig. 4(b) shows the values of 35 AR coefficients for all damage cases. Then MSD values for the three damage cases were calculated by Eq. (2).

Damage monitoring results on the foundation-structure interface are shown in Fig. 5. Damage occurrences of all damages were successfully identified from the variation of MSD value in x-, y-, and z-directions. It was found that MSD values tended to increase according to the increment of damage severities. Also, vibration responses in x- and y-direction were sensitive to the damage growth in the foundation-structure interface.



(a) Partial autocorrelation for undamaged state



(b) Variation of AR coefficients

Fig. 4 Partial autocorrelation and variation of AR coefficients for lab-scale caisson

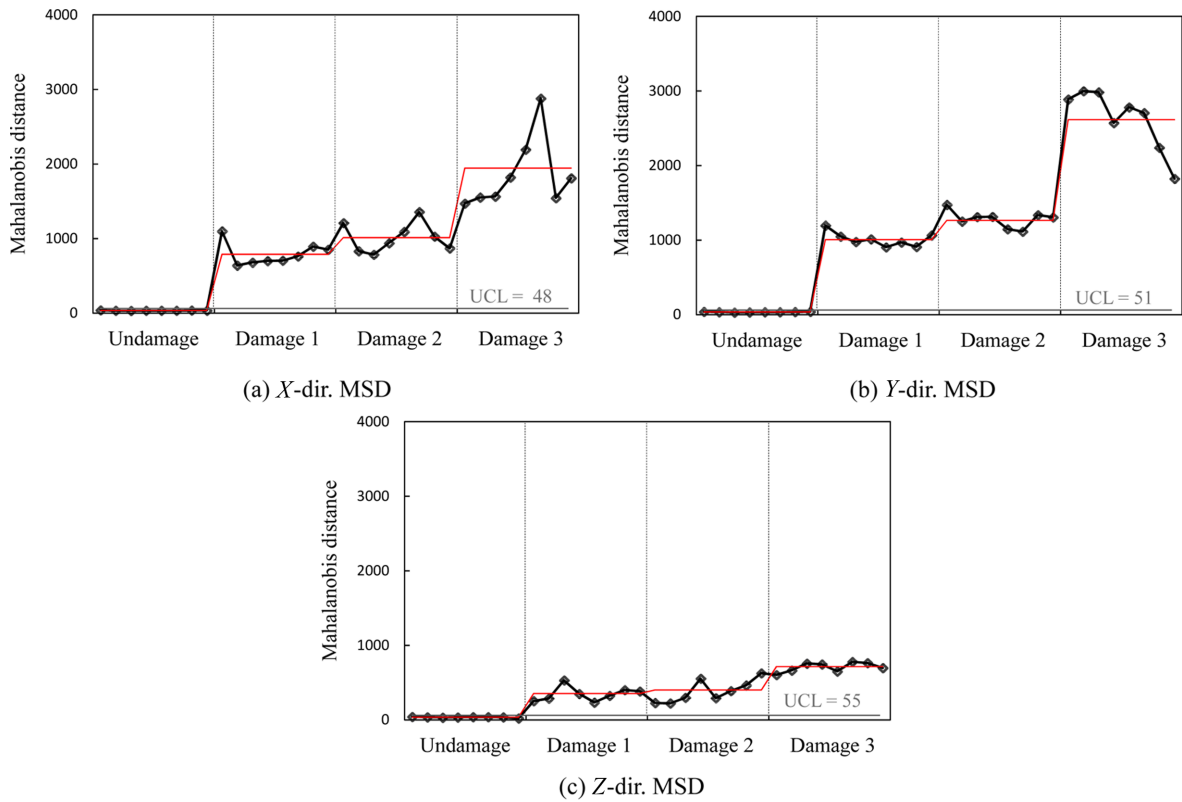


Fig. 5 AR model-based damage monitoring results for lab-scale caisson

3.2.3 PSD-based damage monitoring

In order to verify the PSD-based damage monitoring technique, PSDs of acceleration responses were analyzed by the monitoring scheme as described in Eqs. (4)-(6). Sensor 3(x), Sensor 3(y) and Sensor 3(z) were utilized among 15 sensors shown in Fig. 2(b). In the initialization phase, PSDs of 8 acceleration sets were calculated by Eq. (4) and CC values were calculated by Eq. (5). Based on CC values, LCL was determined by Eq. (6). In the monitoring phase, PSDs of 8 acceleration sets of each damaged state were calculated and CC of PSDs were calculated thereafter. Fig. 6 shows the PSDs of all damage cases. In the figure, PSDs were shifted indicating changes in the caisson system.

Damage monitoring results are shown in Fig. 7. Damage of the foundation-structure interface was exactly detected for all 3 axes. Also, it was observed that the values of CC become reducing due to the damage growth. It was found that the x - and y -directional responses were sensitive to the growth of damage of the foundation-structure interface.

3.2.4 Modal parameter-based damage monitoring

The mode shape-based method requires acceleration data measured from multiple points, so that it can provide information on what modes are sensitive to special damage type or damage location. To specify sensitive vibration modes with respect to the damage of the foundation-structure interface for caisson, natural frequencies and mode shapes of the caisson were analyzed using acceleration data of all 15 sensors.

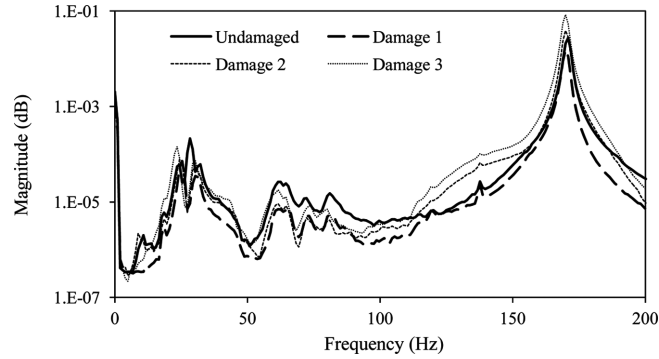


Fig. 6 PSDs of acceleration signals of Sensor 3(y) for lab-scale caisson

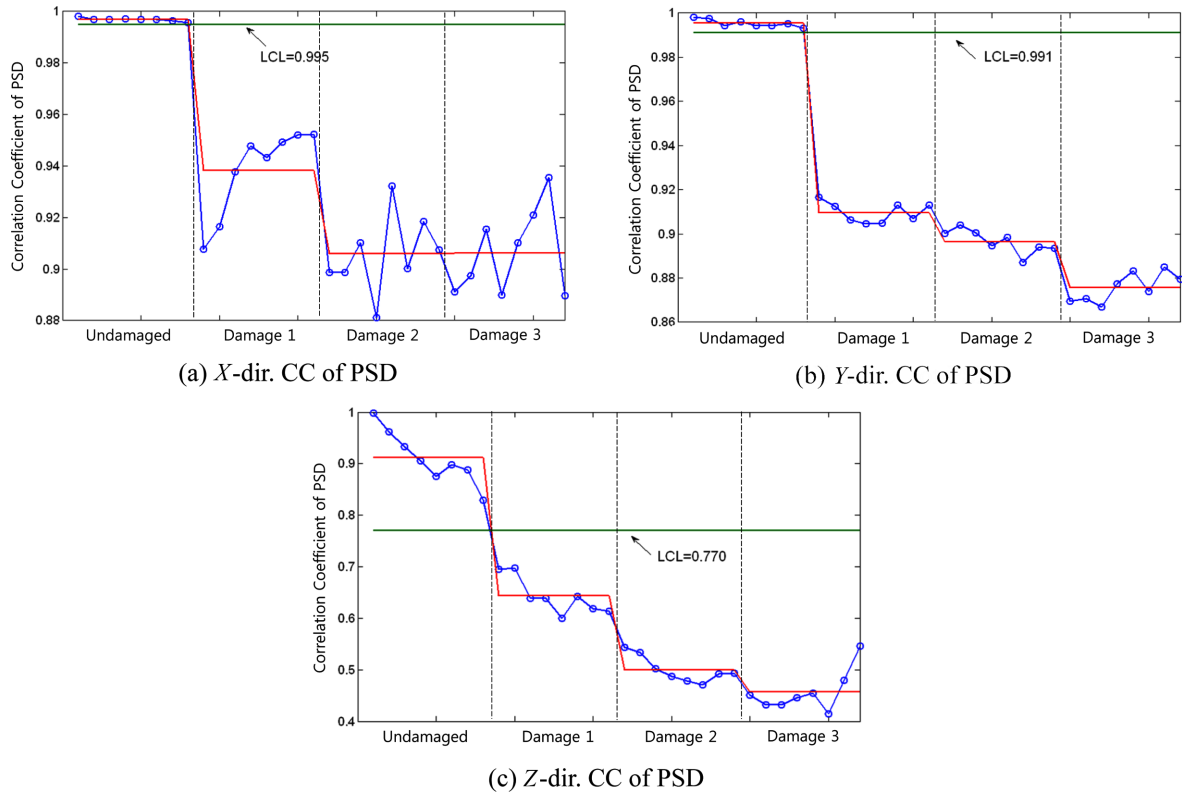


Fig. 7 PSD-based damage monitoring results for lab-scale caisson

As shown in Fig. 8, modal parameters were extracted from the singular values in FDD procedure described in Eq. (7). Among several peaks in frequency range of 0 to 200 Hz, four peaks were selected as the target modes that were 28.32 Hz, 47.85 Hz, 111.33 Hz and 170.90 Hz. Natural frequencies for the damage cases are summarized in Table 1. Due to the damage occurrence, natural frequencies of modes 1 and 3 tended to be increased. On the other hand, frequency decrement due to damage growth was observed for modes 2 and 4.

The mode shapes were extracted from the corresponding peak frequencies as shown in Fig. 9. It

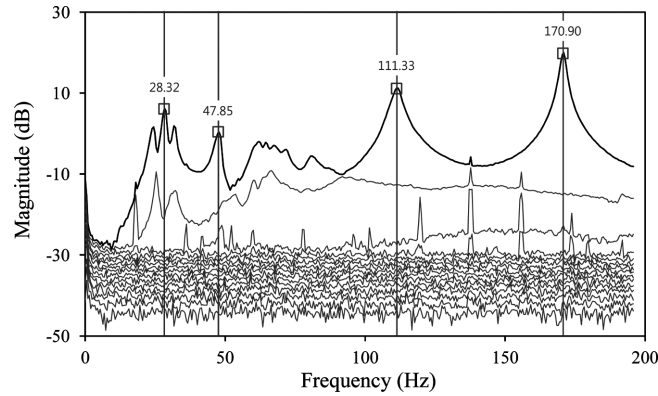


Fig. 8 Singular values of FDD procedure for lab-scale caisson

Table 1 Experimental natural frequencies of lab-scale caisson with foundation damage

Case	Natural frequency (Hz)			
	Mode 1	Mode 2	Mode 3	Mode 4
Undamaged	28.32	47.85	111.33	170.90
Damage 1	29.79 (5.01)	47.85 (0)	112.31 (0.88)	169.92 (-0.57)
Damage 2	29.79 (5.01)	46.88 (-2.03)	112.31 (0.88)	169.92 (-0.57)
Damage 3	29.79 (5.01)	45.41 (-5.10)	112.31 (0.88)	169.92 (-0.57)

*Parentheses indicate variation (%) of natural frequencies with respect to undamaged case

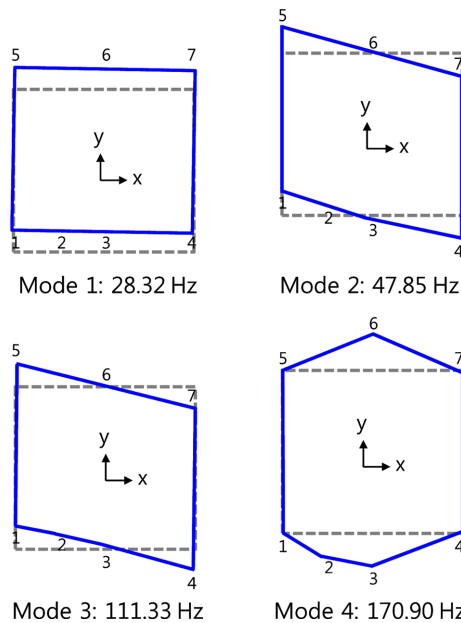


Fig. 9 Natural frequencies and mode shapes of lab-scale caisson

was observed that modes 1 and 2 represented translational and rotational rigid body motions of the caisson, respectively. Meanwhile, modes 3 and 4 represented deformable motions of the caisson

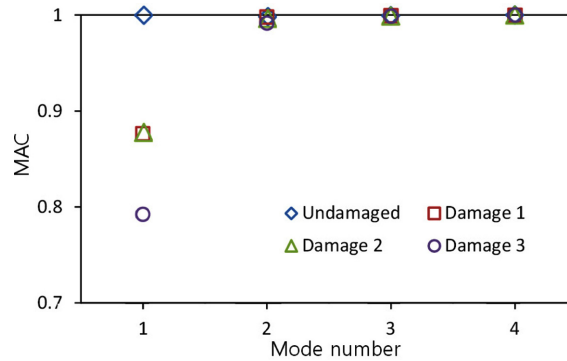


Fig. 10 Experimental MAC values due to foundation damage in lab-scale caisson (a) FE model and (b) plane view

wall. To examine the changes of the four mode shapes due to the foundation damages, the MAC values were calculated by Eq. (8), as shown in Fig. 10. It was observed that the MAC values were reducing due to the damage growth. In the linear relationship between the undamaged and damaged mode shapes, mode 1 (representing the translational rigid body motion) was most sensitive to the foundation-structure interface damage.

4. Numerical examination of damage monitoring

4.1 Finite element models of three caisson types

Even though the vibration features of the lab-scale mono caisson (described in the previous section) were feasible for detecting the occurrence of foundation damage, the feasibility of damage monitoring methods should be examined by considering the real conditions of harbor caisson structures. The first issue is that a harbor caisson structure is partially submerged in the sea water. The second issue is that a whole caisson structure consists of many segments of caisson units. To justify the experimental results with respect to the above-addressed two issues, numerical analyses were carried out for the following three caisson types: (1) Caisson 1 was modeled for the un-submerged mono-caisson with foundation damage; (2) Caisson 2 was modeled for the submerged mono-caisson with foundation damage and water-level change; and (3) Caisson 3 was modeled for the un-submerged interlocked multiple-caissons with foundation damage and interlocking effect. For all numerical models, the material properties were given as listed in Table 2.

4.1.1 FE model of Caisson 1

As shown in Fig. 11, the finite element (FE) model of Caisson 1 in open dry air was designed to

Table 2 Material properties of FE model of caisson structure

	Caisson	Armor gravel	Foundation mound
Mass density (kg/m ³)	2500	2100	2000
Elastic modulus (MPa)	18,000	120	35
Poisson's ratio	0.18	0.3	0.325

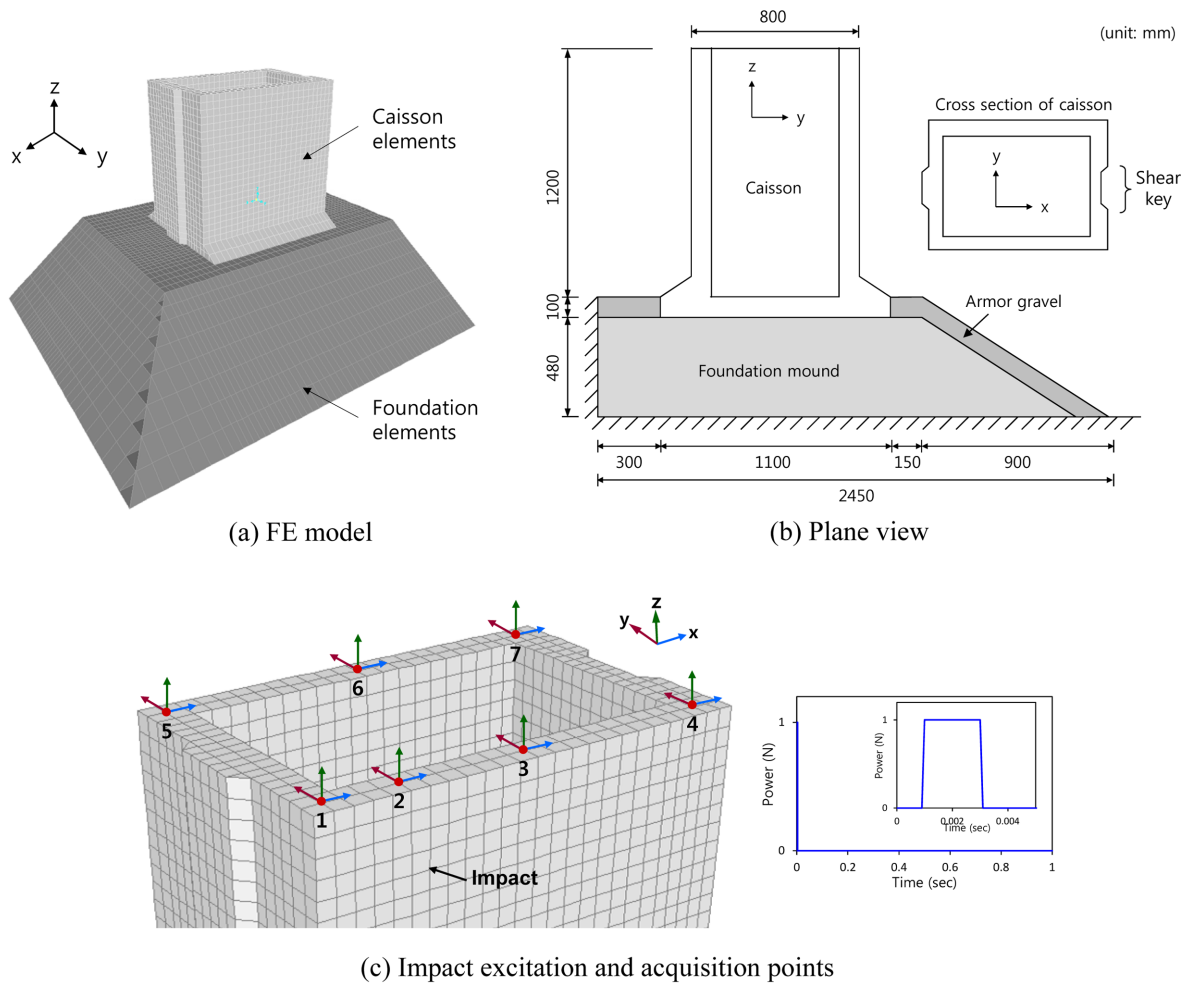


Fig. 11 FE model of un-submerged mono-caisson (Caisson 1)

verify the feasibility of experimental tests on the un-submerged lab-scale caisson structure. Caisson 1 represented the same condition as the experimental tests described previously. It consisted of a reinforced concrete caisson, an armor gravel layer and a foundation mound, as shown in Fig. 11(a) and Fig. 11(b). The caisson stood on the foundation mound covered with the armor gravel layer. The foundation was fixed at the bottom and at two vertical surfaces as shown in Fig. 11(b).

In order to monitor vibration responses of the caisson, forced vibration analysis was designed considering geometrical conditions. An impact force of 1N-power and 0.002s-duration was applied along the corresponding direction to the experimental tests. Three-dimensional acceleration responses were computed at seven points (i.e., points 1-7) on the top of the caisson body as shown in Fig. 11(c). The sampling rate was set as 1 kHz. In order to simulate uncertainties come from environmental effect and measuring condition, five percent of white noise in RMS level was injected into raw acceleration signals. Fig. 12 shows acceleration signals of point 3 in x -, y -, and z -directions. It was observed that the accelerations in y - and z -directions were the largest (about 0.0354 g) and the smallest responses, respectively, as similar to the results of the experimental test.

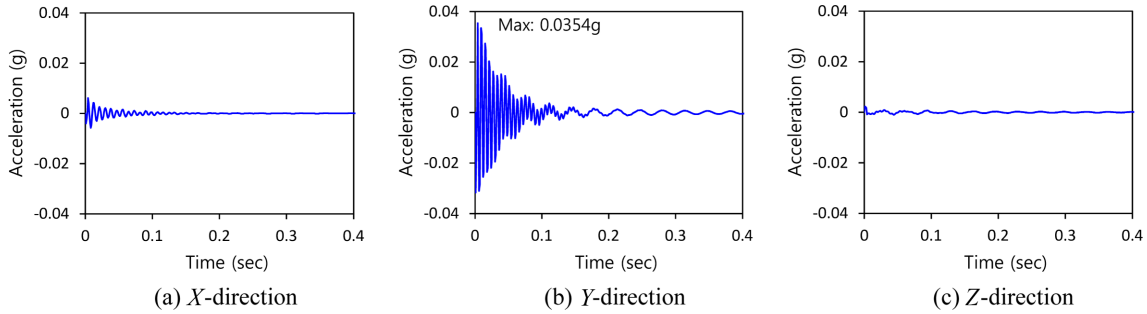


Fig. 12 Numerical acceleration responses of point 3 of Caisson 1

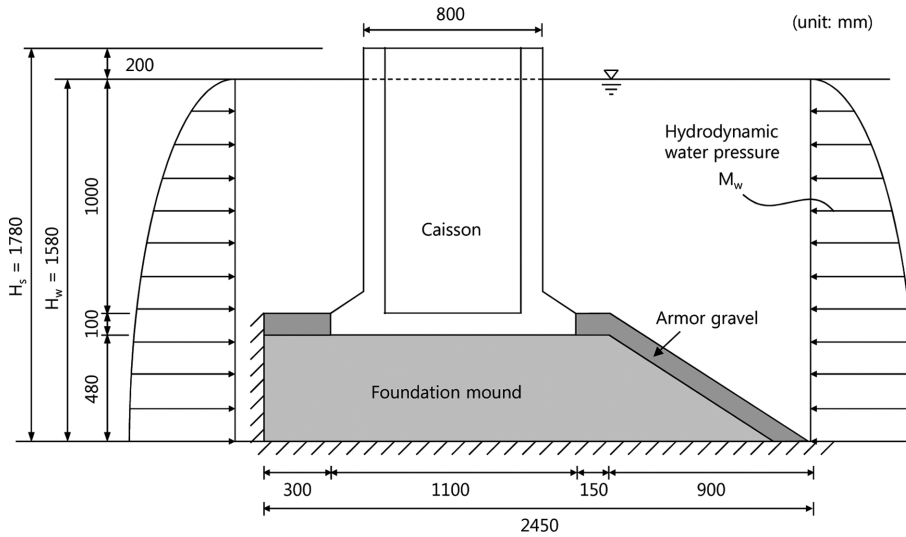


Fig. 13 Hydrodynamic water pressure state for submerged mono-caisson (Caisson 2)

4.1.2 FE model of Caisson 2

As shown in Fig. 13, the FE model of Caisson 2 was designed to examine the effect of submerged condition and water-level change on the feasibility of the damage monitoring methods. The submerged condition was modeled by adding effective mass of water to caisson system. The added mass of water was calculated by Westergaard’s hydrodynamic water pressure equation (Westergaard 1933)

$$M_w = \int_{h_1}^{h_2} \frac{7}{8} \rho \sqrt{H_w \cdot h} \, dh \tag{9}$$

where M_w is the hydrodynamic pressure and ρ is the water density; H_w and h are the depth from the water surface to the foundation and that to the acting point of hydrodynamic pressure, respectively.

To examine the effect of water-level change, two different water-levels were considered. As the reference state, the water-level H_w was set to 89% of the total height H_s (i.e., $H_w/H_s=0.89$) as shown in Fig. 13. Then it was assumed that the water-level rose for a comparative state. The changed water-level was set to 94% of the total height H_s (i.e., $H_w/H_s=0.94$).

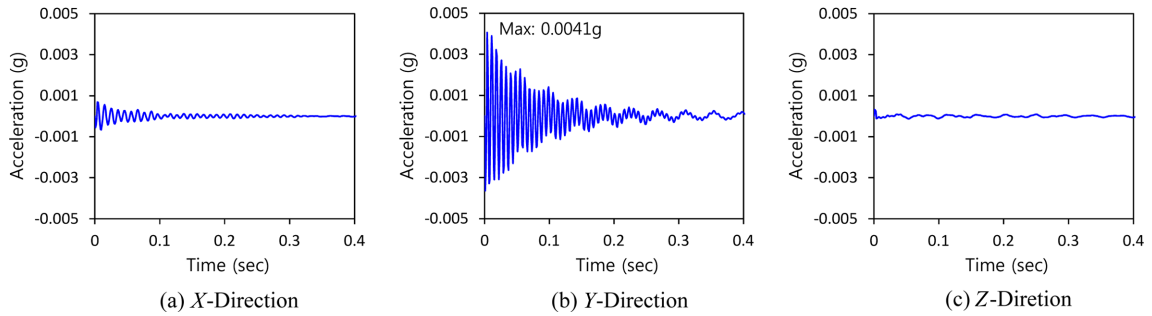


Fig. 14 Numerical acceleration responses of point 3 of Caisson 2 ($H_w/H_s=0.89$)

Numerical vibration responses of Caisson 2 were extracted from forced vibration analysis with the same impact force and data sampling conditions as Caisson 1. Five percent noise was also injected to the raw acceleration signals to simulate the uncertainties. Fig. 14 shows acceleration signals at point 3 in x -, y -, and z -directions for reference water-level. It was observed that the y - and z -directional accelerations were the largest (about 0.0041 g) and the smallest responses. It was also observed that the amplitude of fluctuation is much smaller than that of Caisson 1.

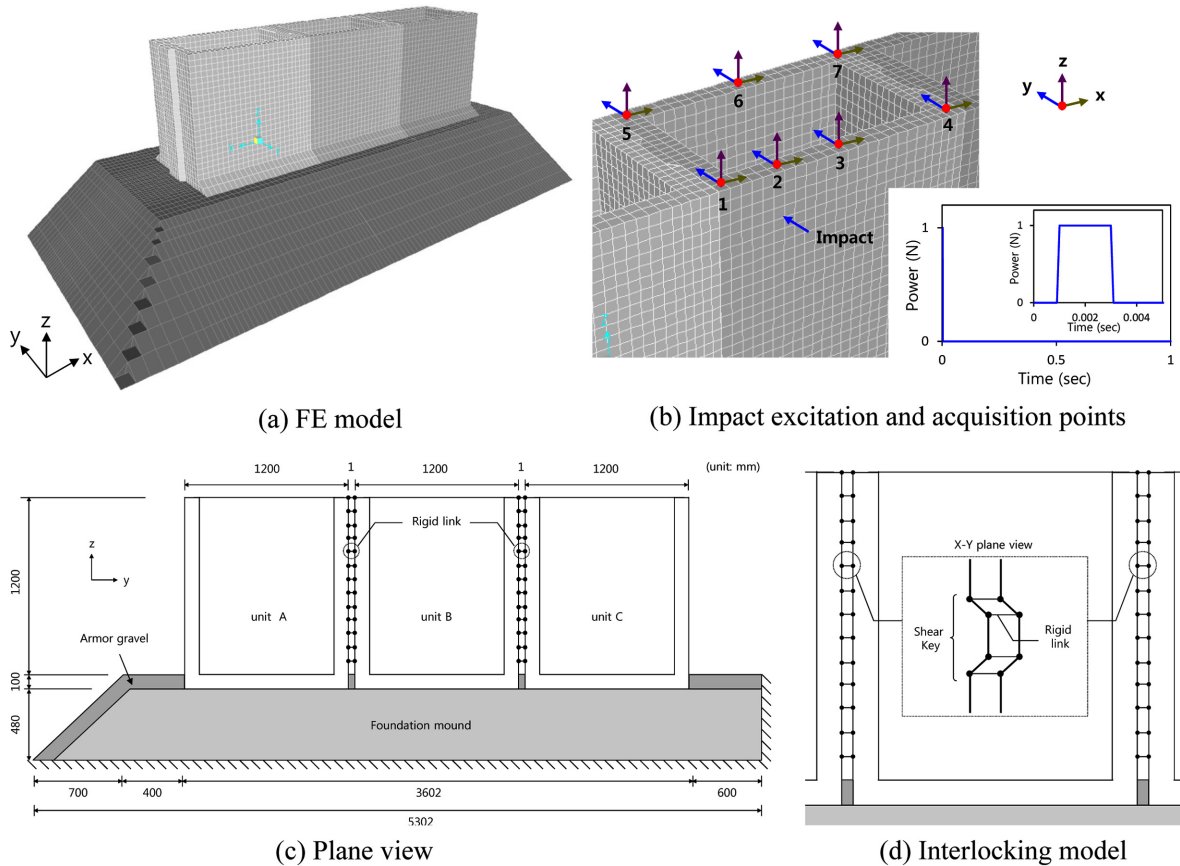


Fig. 15 FE model of un-submerged interlocked multiple-caissons (Caisson 3)

4.1.3 FE model of Caisson 3

As shown in Fig. 15(a), the FE model of Caisson 3 was designed to examine the effect of caisson’s interlocking condition on the feasibility of damage monitoring methods. As shown in Fig. 15(c), Caisson 3 consisted of three units A, B and C to simulate the interlocking behaviors between two adjacent units. As shown in Fig. 15(d), the interlocking was modeled by 2-D rigid links at the shear keys. It was assumed that horizontal vibrations of an individual caisson were propagated to its adjacent caissons.

As shown in Fig. 15(b), the impact excitation was applied to the unit B located in the middle. Acceleration signals were extracted from the seven points in the unit B. Note that the measurement points and sampling rates were the same as the case of Caisson 1. Five percent noise was injected to the raw acceleration signals as the same way as the analysis of Caisson 1. Fig. 16 shows acceleration signals at point 3 in *x*-, *y*-, and *z*-directions. As similar to the analysis of Caisson 1, *y*- and *z*-directional accelerations were the largest (about 0.0013 g) and the smallest. It was also observed that the vibration amplitudes of Caisson 3 were considerably smaller than those of Caisson 1.

4.2 Damage monitoring in three caisson types

4.2.1 Caisson 1 with foundation damage

For Caisson 1, four damage scenarios were simulated in foundation as shown in Fig. 17. The three

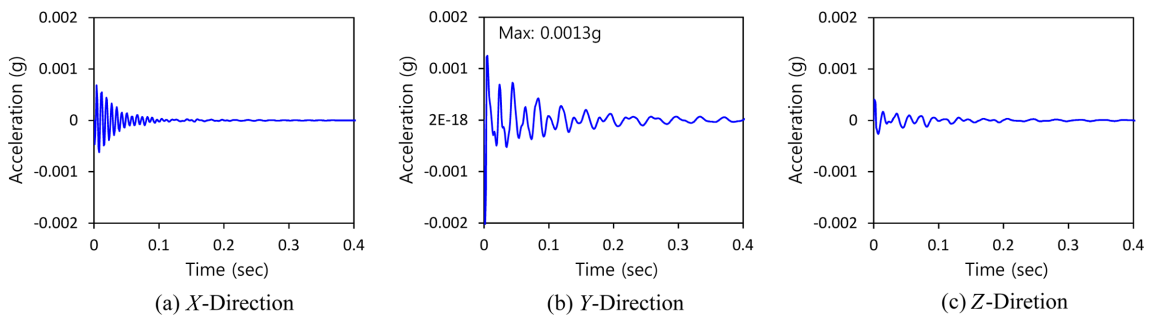


Fig. 16 Numerical acceleration responses of point 3 of Caisson 3

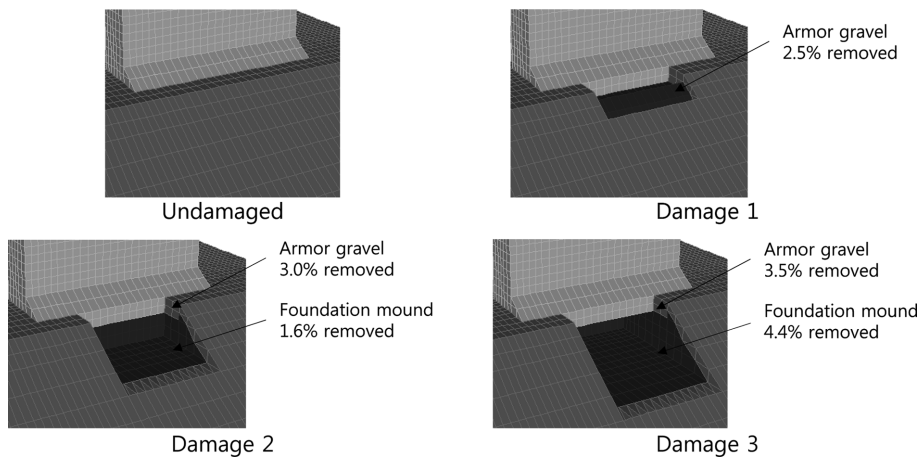


Fig. 17 Damage scenarios simulated in FE models

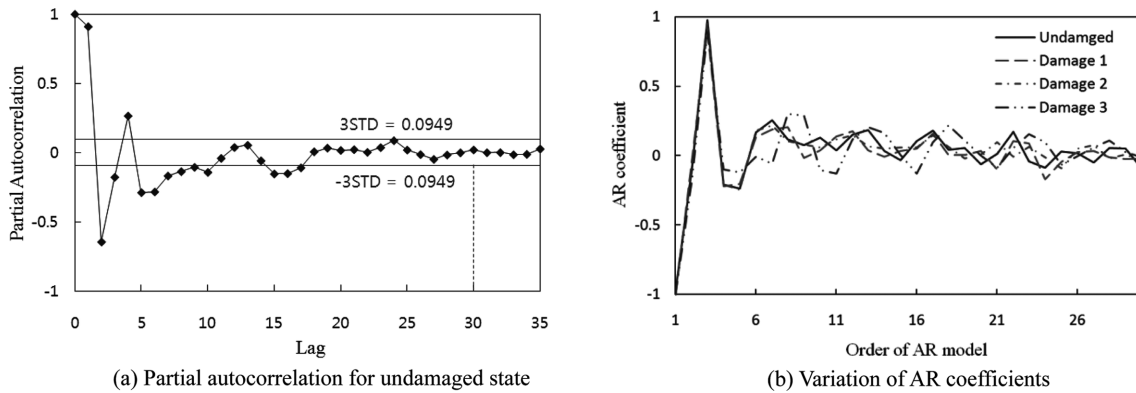


Fig. 18 Partial autocorrelation and variation of AR coefficients for Caisson 1 (injected noise=5%)

damage cases (i.e., Damages 1-3) were almost identical to those of experimental tests as shown in Fig. 3. The damage monitoring of Caisson 1 was performed for the three damage monitoring methods: AR model-based damage monitoring, PSD-based damage monitoring, and modal parameter-based damage monitoring.

4.2.1.1 AR model-based damage monitoring

For AR model-based damage monitoring, acceleration responses of all three axes of point 3 (see Fig. 11(c)) were utilized. The order of AR model was determined by the same way as the laboratory experiment, as described previously. As shown in Fig. 18(a), partial autocorrelation converged into three times of STD (lag 30), so that the order of AR model was determined as 30. Fig. 18(b) shows the variation of the 30 AR coefficients for all damage cases.

The damage monitoring results are shown in Fig. 19. For all damage cases, damage occurrences were successfully identified by using *y*-directional (along the wave action) accelerations. The *x*-directional acceleration responses produced meaningful results for only Damage 3. Meanwhile, it was hard to detect any damage using *z*-directional response. From the analysis, the *y*-directional response (which had the same direction as the incident wave) was most sensitive to damage in foundation-structure interface.

4.2.1.2 PSD-based damage monitoring

The PSDs of acceleration signals in all three axes of point 3 were computed by Eq. (4) for all damage cases, as shown in Fig. 20. In the figure, several large peaks are observed in the range of 0-200 Hz. The peaks of PSD were shifted according to the damage growth. CC of PSD was then calculated by Eq. (5) for damage monitoring. Fig. 21 shows PSD-based damage monitoring results. It was observed that CC values for all three axes were reduced due to the damage growth. It was also found that the *x*- and *y*-directional responses were more sensitive to the damage growth in the foundation-structure interface.

4.2.1.3 Modal parameter-based damage monitoring

To estimate sensitive vibration modes with respect to the damage, modal parameters were obtained from acceleration responses of 7 points on the top of the caisson model (Fig. 11(c)). Natural frequencies were extracted from singular values of FDD procedure (i.e., Eq. (7)) as shown in Fig.

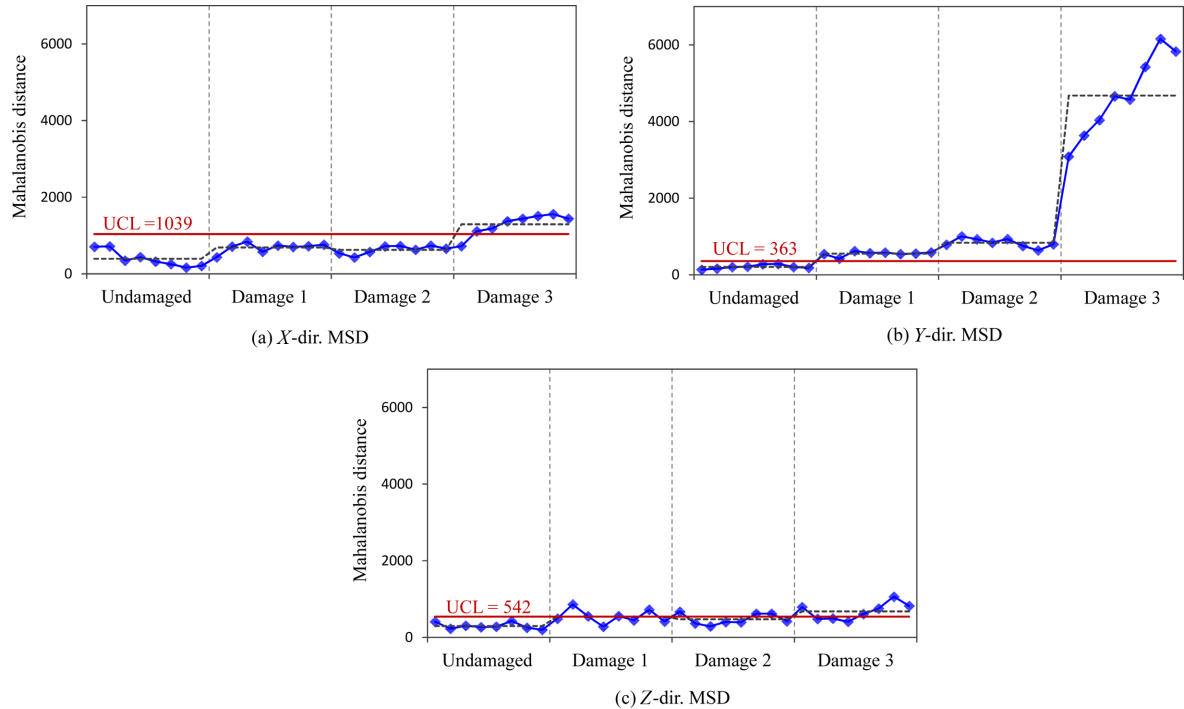


Fig. 19 AR model-based damage monitoring results for Caisson 1 (injected noise=5%)

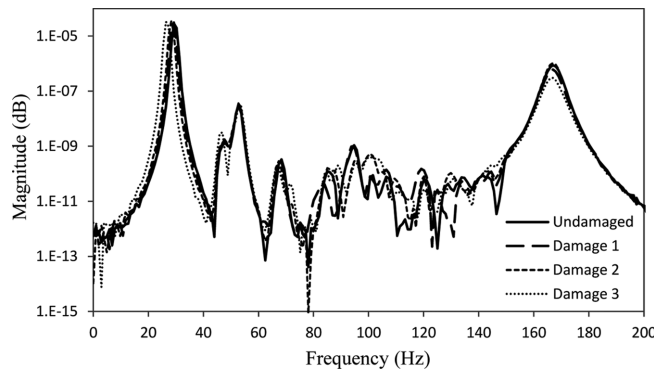


Fig. 20 PSDs of γ -directional acceleration signals of point 3 in Caisson 1

22. Among several peaks in frequency range of 0-200 Hz, four peaks were selected as the target modes that are 29.3 Hz, 68.36 Hz, 116.2 Hz and 167 Hz. Natural frequencies of all damage cases are summarized in Table 3. Natural frequencies of mode 1 and of mode 2 were decreased according to the damage growth. Changes in natural frequencies of modes 3 and 4 are relatively small as less than 1%.

As shown in Fig. 23(a), discrete mode shapes were extracted from the corresponding peak frequencies of Fig. 22. To justify the modal identification, as shown in Fig. 23(b), continuous mode shapes were calculated from free vibration analysis (Note that natural frequencies from the free vibration analysis (Fig. 23(b)) were slightly different from the forced vibration analysis (Fig. 23(a))

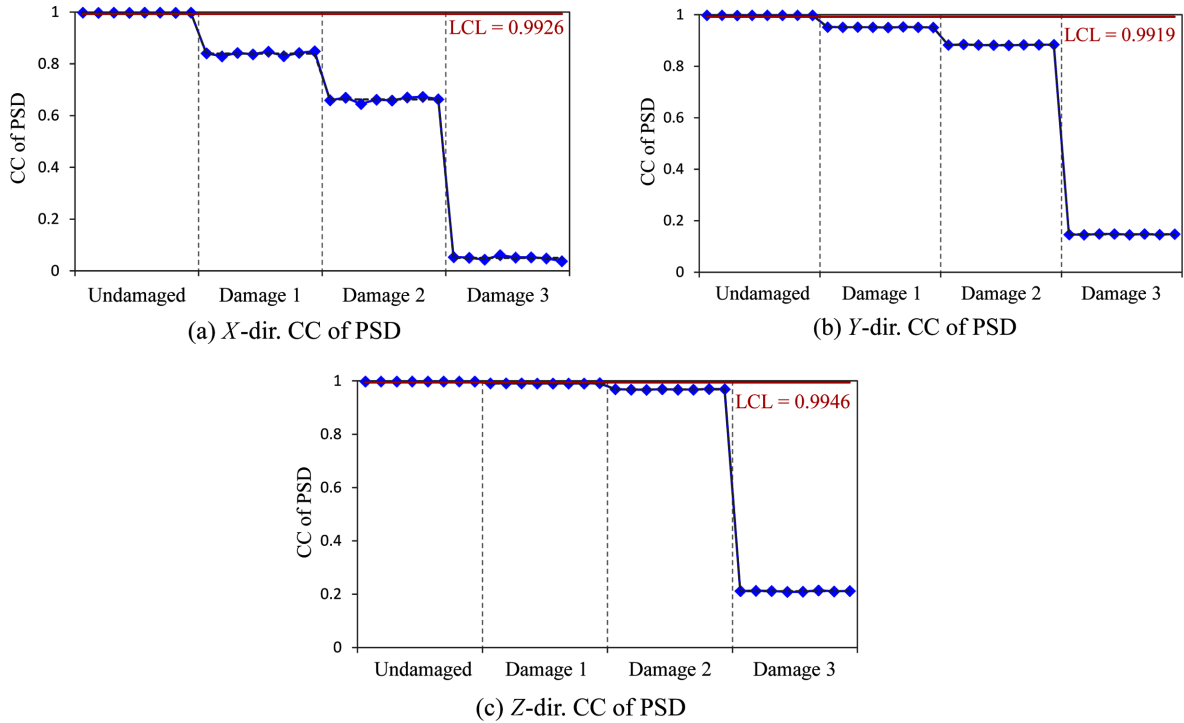


Fig. 21 PSD-based damage monitoring results for Caisson 1 (injected noise=5%)

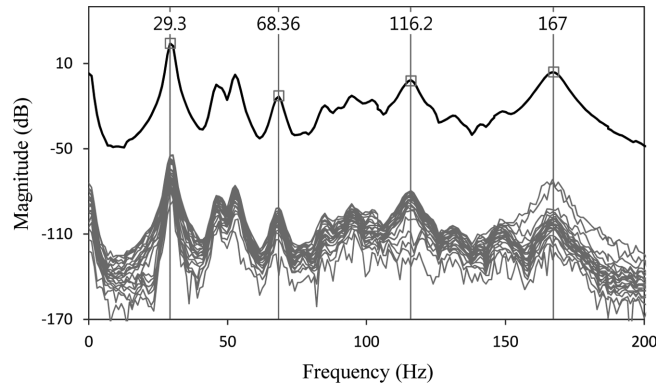


Fig. 22 Singular values of FDD procedure for Caisson 1 (injected noise=5%)

Table 3. Numerical natural frequencies of Caisson 1 with foundation damage

Case	Natural frequency (Hz)			
	Mode 1	Mode 2	Mode 3	Mode 4
Undamaged	29.3	68.36	116.2	167
Damage 1	29.3 (0)	68.36 (0)	115.2 (-0.86)	167 (0)
Damage 2	28.32 (-3.34)	67.38 (-1.43)	116.2 (0)	167 (0)
Damage 3	26.37 (-10.00)	67.38 (-1.43)	117.2 (0.86)	167 (0)

*Parentheses indicate variation (%) of natural frequencies with respect to undamaged case

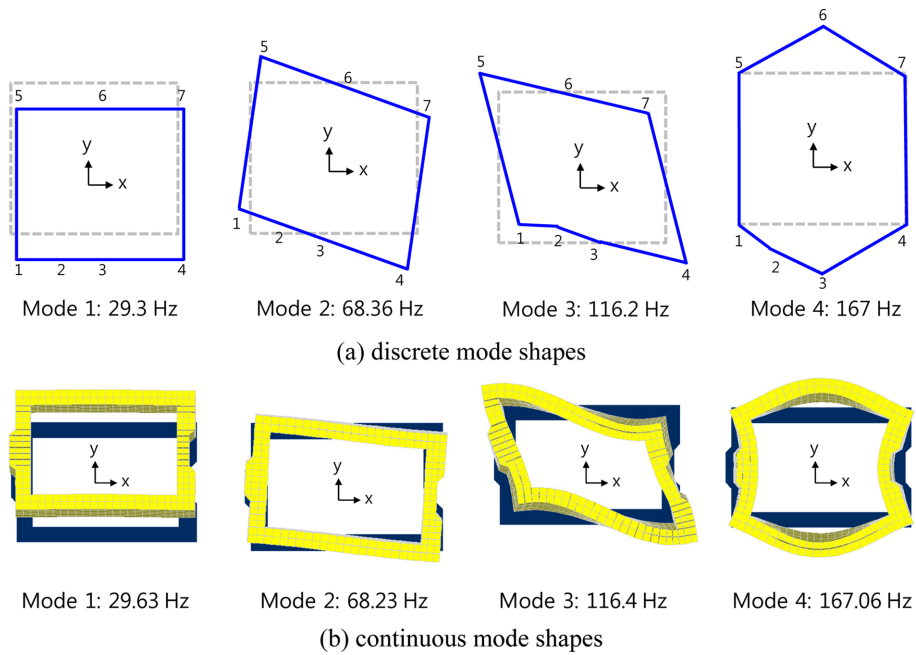


Fig. 23 Numerical mode shapes of Caisson 1

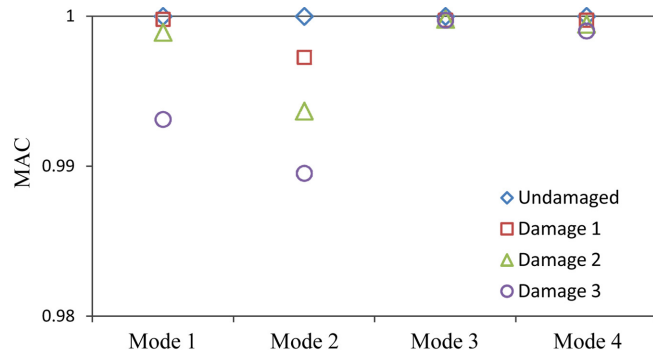


Fig. 24 Numerical MAC values due to foundation damage for Caisson 1 (injected noise=5%)

due to the sampling resolution and the accuracy of modal extraction process). Similar to the lab-scale experiment, modes 1 and 2 represented translational and rotational rigid body motions of the caisson, respectively. Meanwhile, modes 3 and 4 represented deformable motions of the caisson wall. In order to examine the change of mode shape, the MAC values were calculated by Eq. (8), as shown in Fig. 24. It was observed that the MAC values become reducing due to the damage growth. In the linear relationship between the undamaged and damaged mode shapes, mode 2 (which was rotational rigid body mode) was the most sensitive to the foundation-structure interface damage.

4.2.2 Caisson 2 with foundation damage and water-level change

For Caisson 2, foundation damage cases (see Fig. 17) and a water-level change of $H_s/H_w=0.94$ (see Fig. 13) were simulated in the FE model. The effect of the submerged condition on the damage

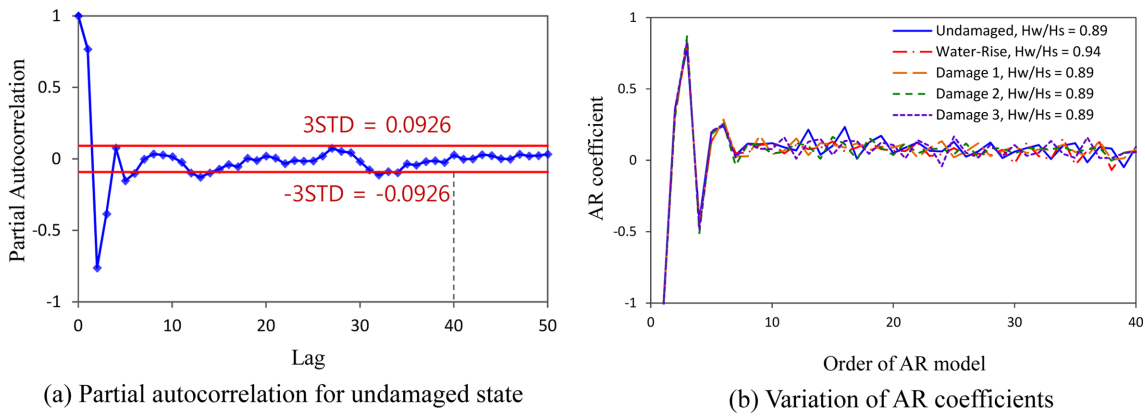


Fig. 25 Partial autocorrelation and variation of AR coefficients for Caisson 2 (injected noise=5%, $H_w/H_s=0.89$)

monitoring in the harbor caisson system was examined as follows.

4.2.2.1 AR model-based damage monitoring

For AR model-based damage monitoring in Caisson 2, y -directional acceleration was selected on the basis of the Caisson 1. From the partial autocorrelation analysis of vibration signal as shown in Fig. 25(a), the order of AR model was determined as 40. In the initialization phase, 50 data sets were used to build up database for reference state. Fig. 25(b) shows the variation of AR coefficients due to damage and water-level change.

Fig. 26 shows AR model-based damage monitoring results. As shown in Fig. 26(a), the MSD values were increased by the damage growth. As shown in Fig. 26(b), the MSD values were also increased by water-level rise. It was observed that the MSD values due to changed water-level ($H_w/H_s=0.94$) were higher than those of the damage cases with reference water-level ($H_w/H_s=0.89$). Therefore, the damage monitoring results based on AR model may be false-positive or false-negative if water-level is changed together with damage occurrence at the same time. Further extensive study is needed to eliminate the effect of water-level change on AR model-based damage detection.

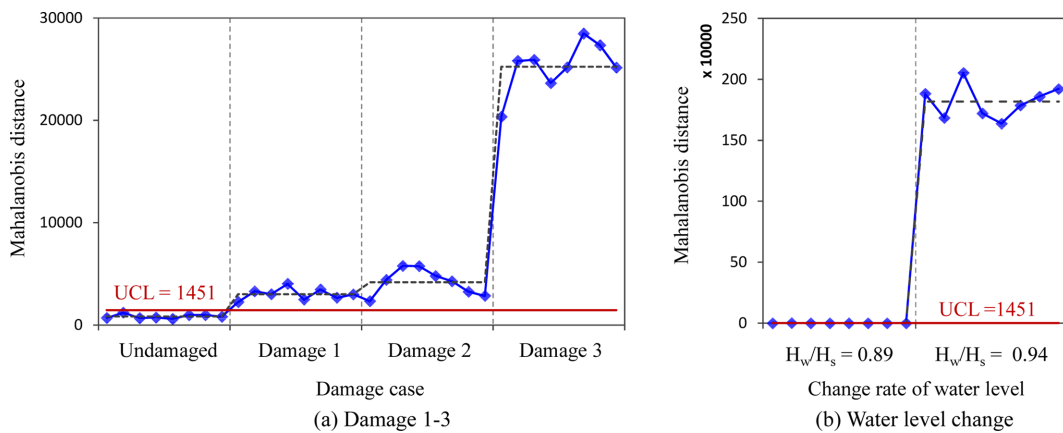


Fig. 26 AR model-based damage monitoring results for Caisson 2 (injected noise=5%)

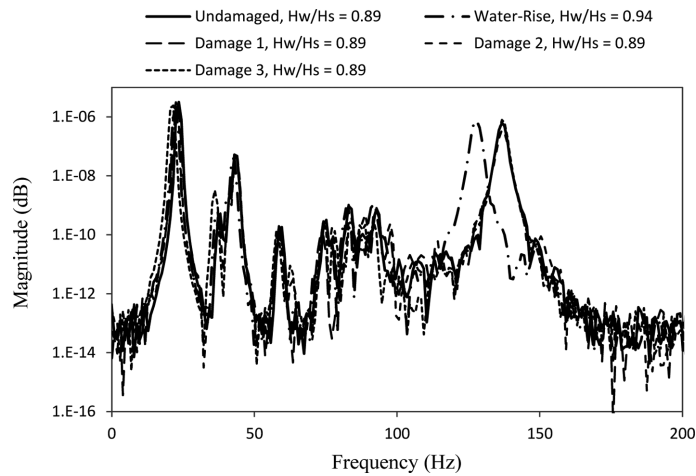


Fig. 27 PSDs of y-directional acceleration signals at point 3 of Caisson 2

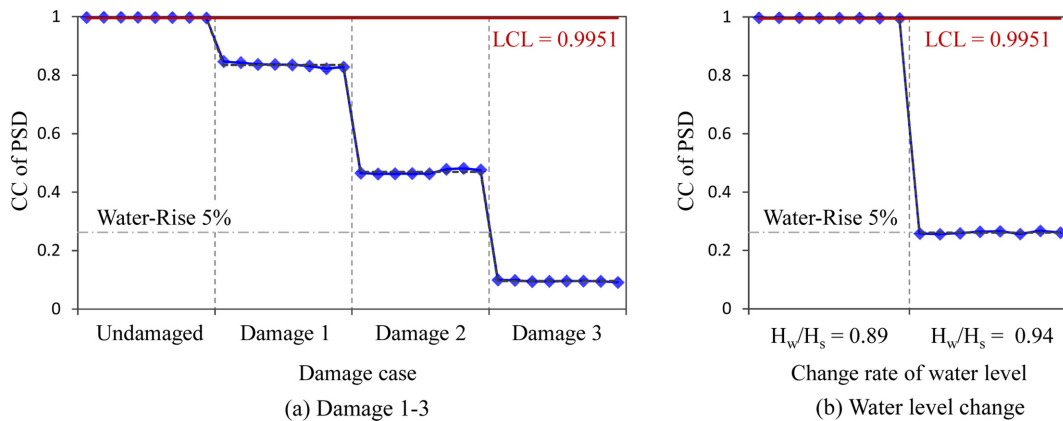


Fig. 28 PSD-based damage monitoring results for Caisson 2 (injected noise=5%)

4.2.2.2 PSD-based damage monitoring

PSDs of each damage level were extracted in the initialization and monitoring phase of PSD-based damage monitoring method. Y-directional acceleration was selected on the basis of the previous Caisson 1 simulation study. Fig. 27 shows the variation of PSD due to damage and water-level change. Due to both inflictions, several peaks in frequency responses were shifted to the lower frequencies.

Fig. 28 shows PSD-based monitoring results due to damage and water-level change. As shown in Fig. 28(a), CC values were gradually decreased due to the occurrence of damage growth. As shown in Fig. 28(b), CC values were also decreased due to the water-level rise. It was observed that the variation due to the 5% water-level change was larger than the variation due to Damage 1 and Damage 2. It meant that PSD-based method might have limitation in damage detection due to the uncertainty in water-level change. Further study is remained to distinguish the effect of water-level change from PSD-based damage detection.

4.2.2.3 Modal parameter-based damage monitoring

Modal parameters were analyzed from Caisson 2. From FDD procedure, singular values were

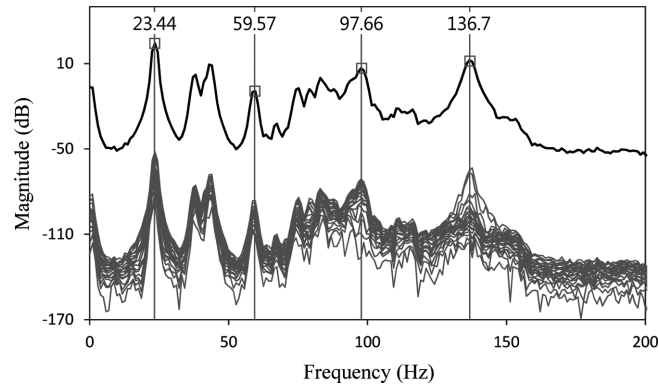

 Fig. 29 Singular values of FDD procedure for Caisson 2 (injected noise=5%, $H_w/H_s=0.89$)

Table 4 Numerical natural frequencies of Caisson 2 with foundation damage and water-level change

Case	H_w/H_s	Natural frequency (Hz)			
		Mode 1	Mode 2	Mode 3	Mode 4
Undamaged	0.89	23.44	59.57	97.66	136.7
Damage 1	0.89	22.46 (-4.18)	58.59 (-1.65)	96.68 (-1.00)	136.7 (0)
Damage 2	0.89	22.46 (-4.18)	58.59 (-1.65)	97.66 (0)	136.7 (0)
Damage 3	0.89	21.48 (-8.36)	57.62 (-3.27)	98.63 (0.99)	136.7 (0)
Water-Rise	0.94	22.46 (-4.18)	58.59 (-1.65)	95.7 (-2.01)	127.9 (-6.44)

*Parentheses indicate variation (%) of natural frequencies with respect to undamaged case

calculated as shown in Fig. 29. In the figure, four target modes were picked at 23.44 Hz, 59.57 Hz, 97.66 Hz and 136.7 Hz. Natural frequencies of all damage cases are summarized in Table 4. Natural frequencies of mode 1 and of mode 2 were decreased due to the damage growth. Changes in modes 3 due to damage were relatively small. For mode 4, there was no change in natural frequency. Meanwhile, natural frequencies of all modes were varied by water-level rise. In rigid-body modes (i.e., mode 1 and mode 2), the five percent water-level rise caused the same amount of changes in natural frequencies as those by Damage 1 and Damage 2. In deformable modes (i.e., mode 3 and mode 4), natural frequencies were considerably decreased by the five percent water-level rise more than by Damage 1 and Damage 2. This implied that the deformable modes 3 and 4 were more sensitive to water-level change compared to the rigid-body modes 1 and 2.

As shown in Fig. 30(a), discrete mode shapes were extracted from the corresponding peak frequencies. For comparative justification, as shown in Fig. 30(b), continuous mode shapes were calculated from free vibration analysis. Similar to the mode shapes of the un-submerged Caisson 1 (Fig. 23), the partially submerged Caisson 2 had a translational mode, a rotational mode and two deformable modes. Then modal parameters were estimated for different water-level and the damage. To examine the change of mode shapes, the MAC values were calculated as shown in Fig. 31. When water-level was changed, MAC values of mode 1 and mode 4 were close to the unity, so that those two modes were not sensitive to the change of water-level. Meanwhile, mode 3 was relatively sensitive to the change of water-level. Also, MAC values were gradually decreased according to the damage growth, especially in mode 2. Damage 3 could be detectable when the water-level was changed by 5%. Despite the effect of water-level change, each mode had different sensitivity to damage in foundation-structure

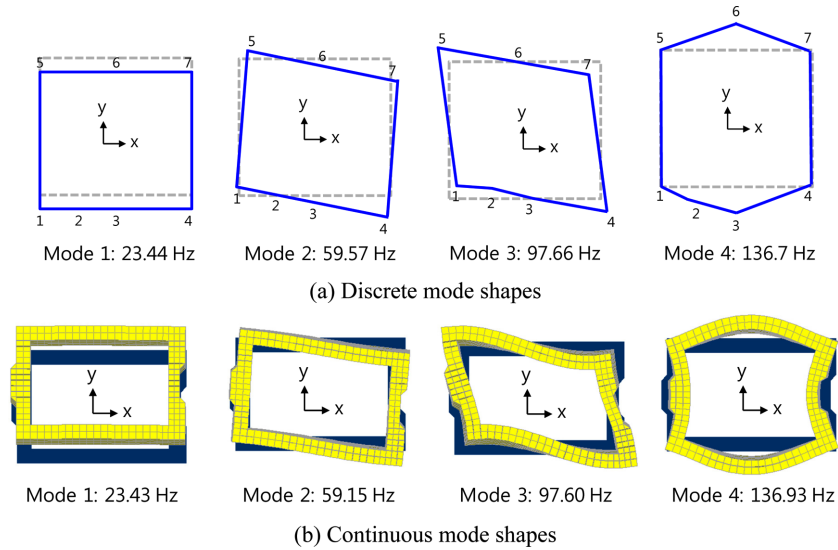


Fig. 30 Numerical mode shapes of Caisson 2 ($H_w/H_s=0.89$)

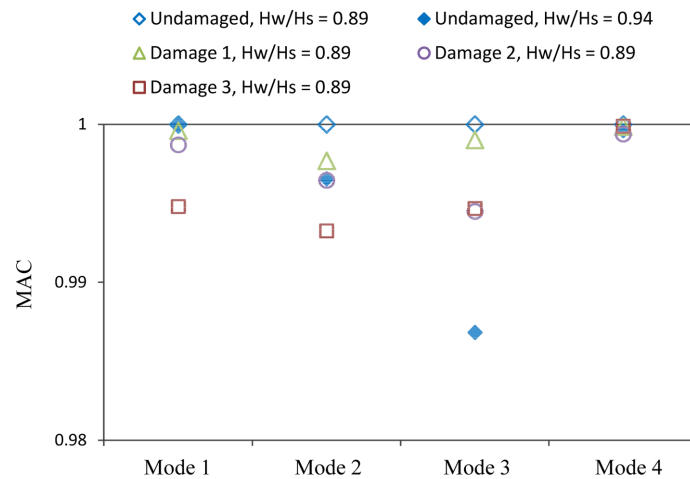


Fig. 31 Numerical MAC values due to foundation damage for Caisson 2 (injected noise=5%)

interface. Thus, the effect of water-level changes may be eliminated by considering the sensitivity of each mode.

4.2.3 Caisson 3 with foundation damage and interlocking effect

For Caisson 3, the same damage scenarios as those of Caisson 1 (see Fig. 17) were simulated in foundation of unit B as shown in Fig. 15(c). The effect of the interlocking condition on the damage monitoring in the un-submerged interlocked multiple-caissons was examined as follows.

4.2.3.1 AR model-based damage monitoring

Acceleration responses of all three axes at point 3 of Fig. 15(b) were utilized for AR model-based damage monitoring. According to the convergence of partial autocorrelation, the order of AR model

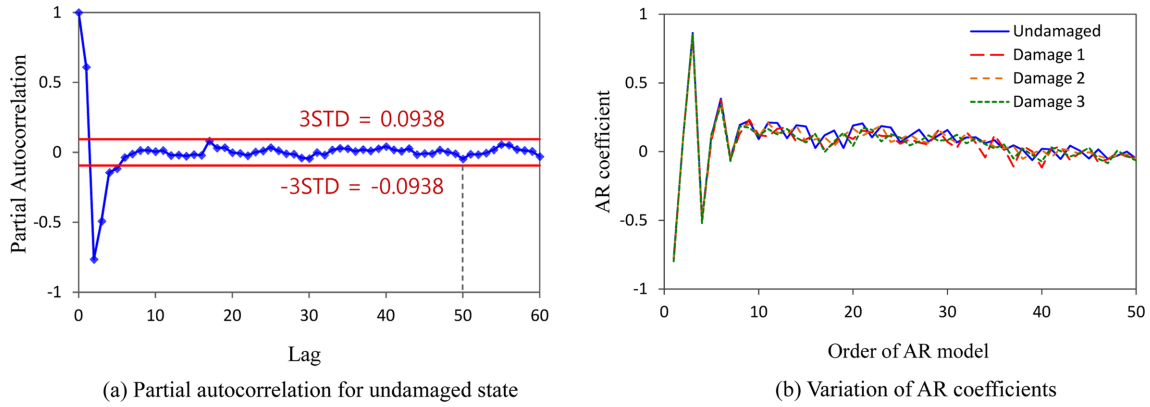


Fig. 32 Partial autocorrelation and variation of AR coefficients for Caisson 3 (injected noise=5%)

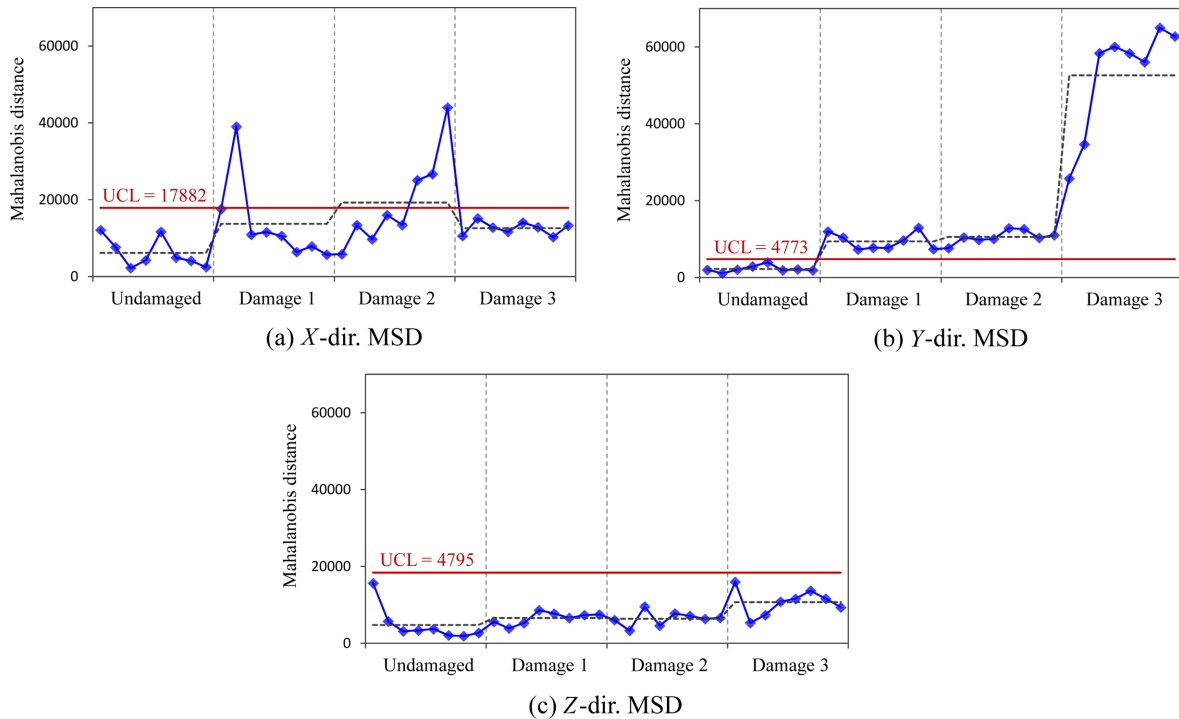


Fig. 33 AR model-based damage monitoring results for Caisson 3 (injected noise=5%)

was selected as 50 as shown in Fig. 32. Then 60 data sets for undamaged stage were used in initialization phase.

Fig. 33 shows AR model-based damage monitoring results of Caisson 3. Using *y*-directional (along the wave action) acceleration responses, the AR model successfully detected all damage scenarios in the caisson units interlocked each other. On the other hand, damage monitoring was not successful by using *x*- and *z*-directional responses. Therefore, the utilization of *x*- and *z*-directional (out of wave action) responses in AR model-based method is not recommended for foundation damage monitoring of caisson structures.

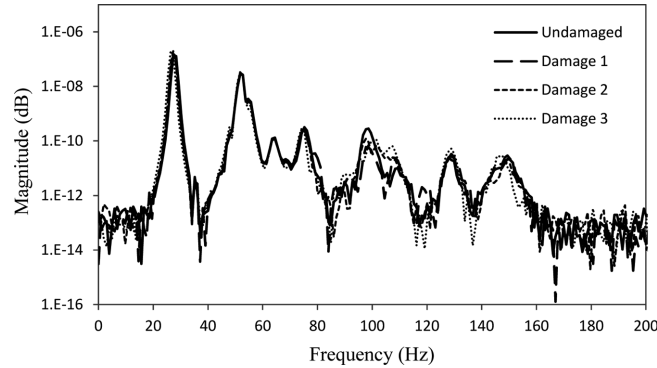


Fig. 34 PSDs of y-directional acceleration signals at point 3 of Caisson 3

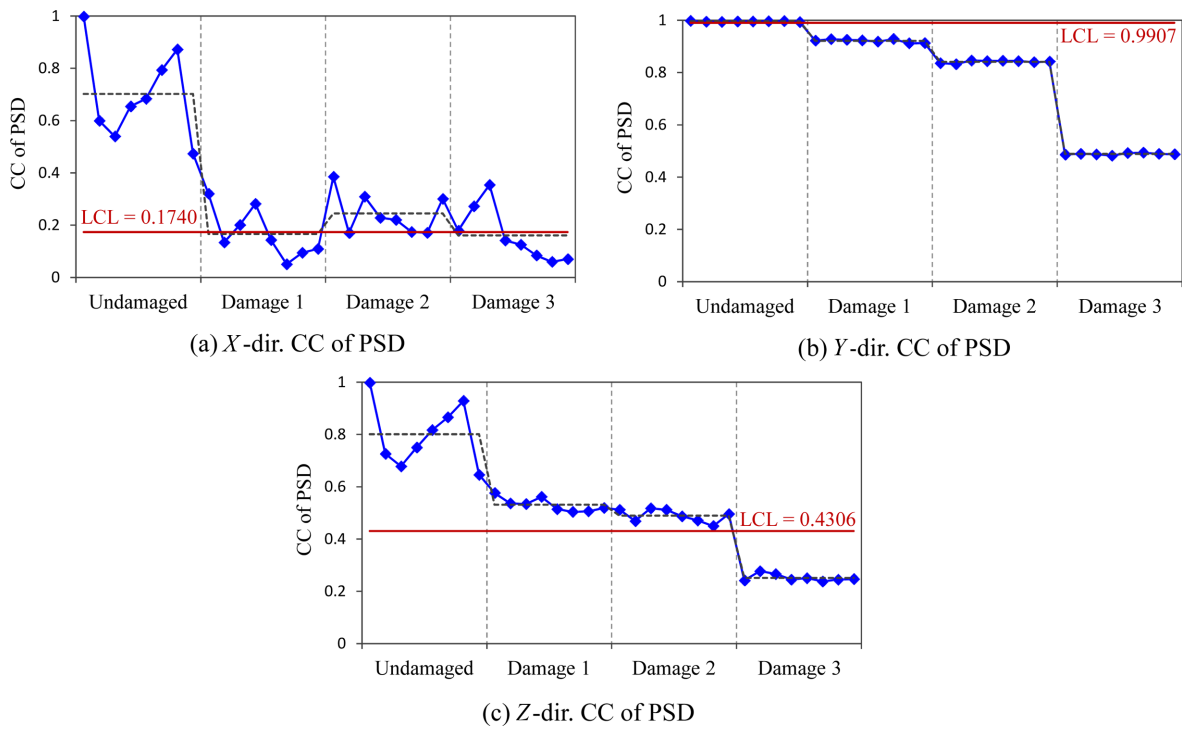


Fig. 35 PSD-based damage monitoring results for Caisson 3 (injected noise=5%)

4.2.3.2 PSD-based damage monitoring

The feasibility of PSD-based damage monitoring for interlocked caisson was also examined. Acceleration responses of all three axes at point 3 (see Fig. 15(b)) were utilized for PSD-based damage monitoring. Fig. 34 shows the change of PSD due to the occurrence of damage growth. It is noted that the first two peaks in the PSDs were similar to those of Caisson 1. Meanwhile, other peaks of PSD were different from those of Caisson 1. From the results, it was observed that the interlocking interaction caused by the shear keys somewhat changed dynamic behaviors in high frequency range.

Fig. 35 shows PSD-based damage monitoring results. Using the y-directional acceleration responses,

the method successfully detected all damage scenarios in the caissons interlocked each other. However, in the results of *x*- and *z*-direction, damage monitoring was not successful. From this result, the utilization of *x*- and *z*-directional responses in PSD-based method is not recommended for foundation damage monitoring of caisson structures.

4.2.3.3 Modal parameter-based damage monitoring

Fig. 36 shows the singular values of FDD procedure to extract modal parameters for Caisson 3. The first four modes (28.32 Hz, 52.73 Hz, 68.36 Hz and 128.9 Hz) were selected as the target modes. For all damage scenarios, natural frequencies of Caisson 3 are listed in Table 5. It was observed that natural frequencies of mode 1 and mode 2 were much decreased due to the damage growth. Meanwhile, natural frequencies of modes 3 and 4 were little changed due to damage growth. These results were identical to those of Caisson 1.

As shown in Fig. 37(a), discrete mode shapes were extracted from the corresponding peak frequencies. For justification, continuous mode shapes obtained from free vibration analysis are shown in Fig. 37(b). Caisson 3’s mode 1 represented translational motion and it was similar to Caisson 1’s mode 1 (see Fig. 23). Meanwhile, Caisson 3’s mode 2 represented a combination of translational and rotational motions and it was different from Caisson 1’s mode 2. Also, modes 3 and 4 of Caisson 3 represented deformable motions which were similar to those of Caisson 1, but different in order. For the four selected modes, MAC values were calculated for all damage scenarios as shown in Fig. 38. Observing the rigid body modes with respect to the damage growth, it was found that MAC values of mode 2 were gradually decreased while MAC values of mode 1 were little affected by the foundation damages. These results were similar to those obtained from

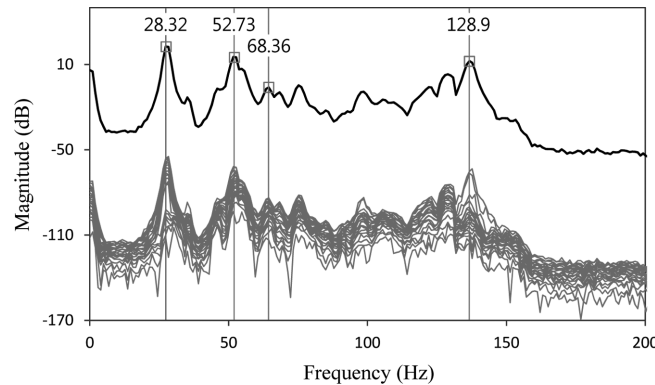


Fig. 36 Singular values of FDD procedure for Caisson 3 (injected noise=5%)

Table 5 Numerical natural frequencies of Caisson 3 with foundation damage

Case	Natural frequency (Hz)			
	Mode 1	Mode 2	Mode 3	Mode 4
Undamaged	28.32	52.73	68.36	128.9
Damage 1	27.34 (-3.46)	51.76 (-1.84)	68.36 (0)	128.9 (0)
Damage 2	27.34 (-3.46)	51.76 (-1.84)	68.36 (0)	127.9 (-0.78)
Damage 3	26.37 (-6.89)	51.76 (-1.84)	68.36 (0)	127.9 (-0.78)

*Parentheses indicate variation (%) of natural frequencies with respect to undamaged case

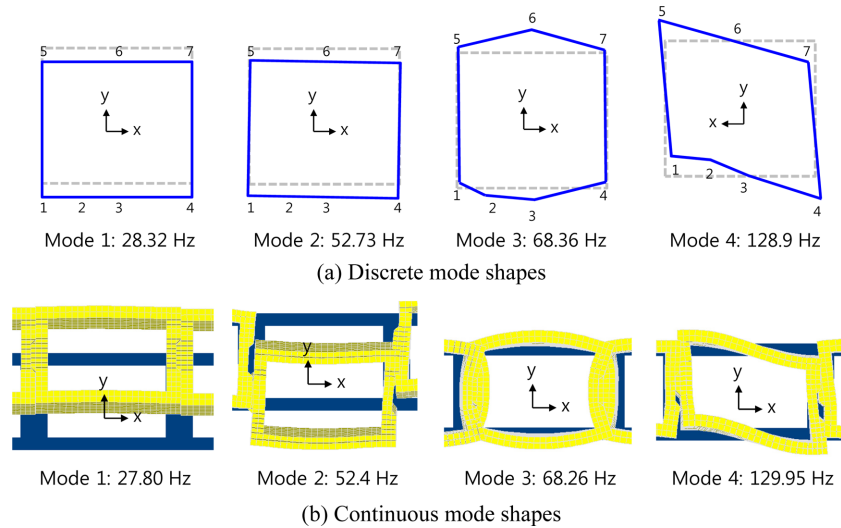


Fig. 37 Numerical mode shapes of Caisson 3

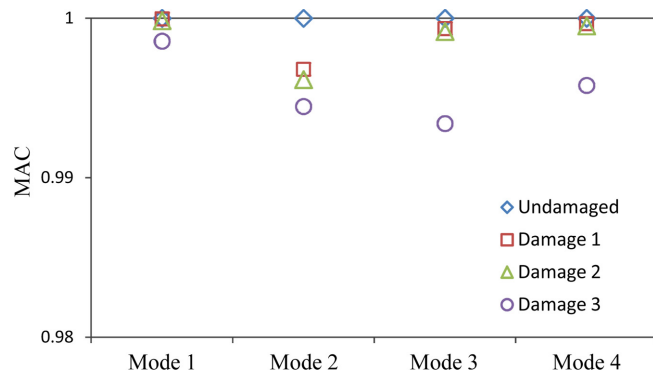


Fig. 38 Numerical MAC values due to foundation damage for Caisson 3 (injected noise=5%)

Caisson 1. By observing the deformable mode shapes (mode 3 and 4), it was found that they were almost unchanged due to the damages in armor gravel layer (i.e., Damage 1 and Damage 2). These results were also similar to the analysis of Caisson 1. For Damage 3, however, a significant change was observed in those mode shapes. Then it is concluded that the utilization of mode 2 promises the most accurate results in modal parameter-based method for damage monitoring.

5. Conclusions

In this paper, vibration-based methods to monitor damage in foundation-structure interface of harbor caisson structure were presented. For harbor caisson structures, vibration-based damage monitoring methods were selected as follows: autoregressive model and correlation coefficient of power spectral density, and modal parameters. The feasibility of the damage monitoring methods was experimentally examined by lab-scale un-submerged mono-caisson. Numerical analyses of un-

submerged mono-caisson, submerged mono-caisson and un-submerged interlocked multiple-caissons were also carried out to examine the effect of boundary-dependent parameters on the damage monitoring of harbor caisson structures.

The following observations and conclusions have been made. The proposed vibration-based damage monitoring methods were successful at detecting damage to the foundation-structure interface of the caisson in various conditions. Although the submerged and interlocking conditions affected the dynamic behaviors of the caisson structure, the proposed methods were still able to detect the damages in foundation-structure interface. Also, the damage growth was realized by the patterns of Mahalanobis- squared-distance (MSD) of AR coefficients, CC of PSD and MAC value. Specifically, it was found that dynamic behaviors of foundation-structure subsystem were the mixtures of rigid body motions and deformable motions. Among those, rigid body motions were more sensitive to the damage.

Despite the feasibility of the proposed vibration-based methods for detecting damages in foundation-structure interface, several issues were identified that need to be resolved. First, the effect of water-level change on the damage monitoring results was quite big. Therefore, additional methods to eliminate the water-level effect should be studied extensively. Next, the sensitivities of numerical mode shapes due to damage were not identical to those of experiments. Future efforts to improve the accuracy of numerical simulation are needed to better represent dynamic behavior of the caisson structure. Obtaining quantitative estimates of the sensitivities of rigid body modes (translation and rotation) to the damage is also remains as topic for future study.

Acknowledgements

This work was supported by Basic Science Research Program through the National Research Foundation of Korea (NRF) funded by the Ministry of Education, Science and Technology (2011-0004253). The authors also would like to acknowledge the financial support of the project 'Development of inspection equipment technology for harbor facilities' funded by Korea Ministry of Land, Transportation, and Maritime Affairs.

References

- Allen, R.T.L. (1998). *Concrete in coastal structures*, Thomas Telford, London.
- Atkan, A.E., Farhey, D.N., Helmicki, A.J., Brown, D.L., Hunt, V.J., Lee, K.L. and Levi, A. (1997), "Structural identification for condition assessment: experimental arts", *J. Struct. Eng. - ASCE*, **123**(12), 1674-1684.
- Bendat, J.S. and Piersol, A.G. (2003), *Engineering applications of correlation and spectral analysis*, Wiley-Interscience, New York, NY.
- Boroschek, R.L., Baesler, H. and Vega, C. (2011), "Experimental evaluation of the dynamic properties of a wharf structure", *Eng. Struct.*, **33**(2), 344-356.
- Brownjohn, J.M.W., Xia, P.Q., Hao, H. and Xia, Y. (2001), "Civil structure condition assessment by FE model updating: methodology and case studies", *Finit. Elem. Anal. Des.*, **37**(10), 761-775.
- Catbas, F.N., Gul, M. and Burkett, J. (2008), "Conceptual damage-sensitive features for structural health monitoring: laboratory and field demonstrations", *Mech. Syst.Signal Pr.*, **22**(7), 1650-1669.
- Doebbling, S.W., Farrar, C.R. and Prime, M.B. (1998), "A summary review of vibration-based damage identification method", *Shock Vib.*, **30**(2), 91-105.
- Ewins, D.J. (2000), *Modal testing: theory, practice and application*, Research Studies Press LTD., Hertfordshire,

UK.

- Isemoto, R., Kim, C.W., Sugiura, K. and Kawatani, M. (2011), "Autoregressive coefficients as an indicator for abnormality detection of bridges", *Proceedings of the 2011 world Congress on Advances in Structural Engineering and Mechanics*, Seoul, Korea, September.
- Jang, S.A., Jo, H., Cho, S., Mechtov, K.A., Rice, J.A., Sim, S.H., Jung, H.J., Yun, C.B., Spencer, Jr., B.F., and Agha, G. (2010), "Structural health monitoring of a cable-stayed bridge using smart sensor technology: deployment and evaluation", *Smart Struct. Syst.*, **6**(5-6), 439-459.
- Kim, D.K., Ryu, H.R., Seo, H.R. and Chang, S.K. (2005), "Earthquake response characteristics of port structure according to exciting frequency components of earthquakes (in Korean)", *J. Korean Soc. Coast.Ocean Eng.*, **17**(1), 41-46.
- Kim, J.T. and Stubbs, N. (1995), "Model-uncertainty impact and damage-detection accuracy in plate girder", *J. Struct. Eng.- ASCE*, **122**(10), 1409-1417.
- Kwon, S.J. and Shin, S (2006), "Determination of optimal acceleration locations with verification by frequencydomain SI method", *Proceedings of the US-Korea Workshop on Smart Structures Technology for Steel Structures*, Seoul, Korea, November.
- Lee, S.Y., Lee, S.R., Kim, J.T. and Yi, J.H. (2011), "Vibration-based monitoring of caisson-type breakwater with damaged foundation-structure interface", *Proceedings of the 2011 World Congress on Advances in Structural Engineering and Mechanics*, Seoul, Korea, September.
- Levin, R.J and Lieven, N.A.J. (1998), "Dynamic finite element model updating using simulated annealing and genetic algorithms", *Mech. Syst. Signal Pr.*, **12**(1), 91-120.
- Otte, D., Van de Ponsele, P. and Leuridan, J. (1990), "Operational shapes estimation as a function of dynamic loads", *Proceedings of the 8th International Modal Analysis Conference*, Florida, USA, January.
- Shi, Z.Y., Law, S.S. and Zhang, L.M. (1998), "Structural damage localization from modal strain energy change", *J. Sound Vib.*, **285**(5), 825-844.
- Sohn, H. and Farrar, C. (2001), "Damage diagnosis using time series analysis of vibration signals", *Smart Mater. Struct.*, **10**(3), 446-451.
- Wang, Y.Z., Chen, N.N. and Chi L.H. (2006) "Numerical simulation on joint motion process of various modes of caisson breakwater under wave excitation", *Commun. Numer. Meth. En.*, **22**(6), 535-545.
- Westergaard, H.M. (1933) "Water pressures on dams during earthquakes", *T. Am. Soc.*, **98**(2), 418-432.
- Wu, X, Ghaboussi, J. and Garret, J.H., Jr. (1992), "Use of neural networks in detection of structural damage", *Comput. Struct.*, **42**(4), 649-659.
- Yang, Z., Elgamal, A., Abdoun, T. and Lee, C.J. (2001), "A numerical study of lateral spreading behind a caisson-type quay wall", *Proceedings of the 4th International Conference on Recent Advances in Geotechnical Earthquake Engineering and Soil Dynamics and Symposium*, California, USA, March.
- Yi, J.H. and Yun, C.B (2004), "Comparative study on modal identification methods using output-only information", *Struct. Eng. Mech.*, **17**(3-4), 445-456.
- Yun G.J., Ogorzalek, K.A., Dyke, S.J. and Song, W. (2009), "A two-stage damage detection approach based on subset of damage parameters and genetic algorithms", *Smart Struct. Syst.*, **5**(1), 1-21.
- Yun, C.B. and Bahng, E.Y. (2000), "Substructural identification using neural networks", *Comput. Struct.*, **77**(1), 41-52.